Stockholms universitet

Synthesis and modification of potential CO_2 adsorbents

-Amine modified silica and calcium carbonates

BAROZ AZIZ

Department of Materials and Environmental Chemistry
Stockholm University

Dedicated to mum and dad

Abstract

The prospect of rapid changes to the climate due to global warming is subject of public concern. The need to reduce the emissions of atmospheric green house gases and in particular carbon dioxide is greater than ever. Extensive research is performed to find new solutions and new materials, which tackles this problem in economically benign way. This thesis dealt with two potential adsorbents for post combustion carbon capture, namely, amine modified silica and calcium carbonates. We modified porous silica with large surface area by propyl-amine groups to enhance the carbon dioxide adsorption capacity and selectivity. Experimental parameters, such as reaction time, temperature, water content, acid and heat treatment of silica substrate were optimized using a fractional factorial design. Adsorption properties and the nature of formed species upon reaction of CO_2 and amine-modified silica were studied by sorption and infrared spectroscopy. Physisorbed and chemisorbed amount of adsorbed CO_2 were, for the first time, estimated directly in an accurate way. The effects of temperature and moisture on the CO_2 adsorption properties were also studied.

Crystallization of calcium carbonate as a precursor to calcium oxide, which can be used as carbon dioxide absorbent, was studied in the second part of this thesis. Structure of different amorphous phases of calcium carbonate was studied in detail. Crystallization of calcium carbonate with and without additives was studied. Parameters like stirring rate, temperature, pH and polymer concentration showed to be important in selection of phase and morphology. An aggregation mediated crystallization was postulated to explain the observed morphologies.

List of publications

Paper I.

Baroz Aziz, Guoying Zhao and Niklas Hedin.

Carbon Dioxide Sorbents with Propylamine Groups-Silica Functionalized with a Fractional Factorial Design Approach

Langmuir, 27 **(2011),** issue 7, pages 3822-3834.

Paper II.

Guoying Zhao, **Baroz Aziz** and Niklas Hedin.

Carbon dioxide adsorption on mesoporous silica surfaces containing amine-like motifs

Applied Energy, 87 **(2010),** pages 2907–2913.

Paper III.

Baroz Aziz, Niklas Hedin and Zoltan Bacsik.

Quantification of Chemisorption and Physisorption of Carbon Dioxide on Porous Silica Modified by Propylamines: Effect of Amine Density
Microporous & Mesoporous Material.
Accepted by the Journal of Microporous & Mesoporous Materials. **(2012) DOI:** 10.1016/j.micromeso.2012.04.007

Paper IV.

Baroz Aziz, Denis Gebauer and Niklas Hedin.

Kinetic control of particle-mediated calcium carbonate crystallization

Crystengcomm, 13 **(2011),** issue 14, pages 4641-4645.

Paper V.

Gebauer, Denis; Gunawidjaja, Philips N.; Ko, J. Y. Peter; Bacsik, Zoltan; **Baroz Aziz**; Liu, Lijia; Hu, Yongfeng; Bergstrom, Lennart; Tai, Cheuk-Wai; Sham, Tsun-Kong; Eden, Mattias and Hedin, Niklas.

Proto-Calcite and Proto-Vaterite in Amorphous Calcium Carbonates

Angewandte Chemie 19 **(2010)** issue 47, pages 8889-8891.

Contributions to the papers:

Paper II: Modification of the adsorbents, surface area, some CO_2 adsorption measurements and thermal analysis as well as intellectual discussion.

Paper V: Minor contribution in form of Scanning electron microscopy measurements adsorption measurements (not presented) as well as discussion.

Table of Contents

Introduction

A reality that we are faced with today is that our global climate is changing. We observe a rapid increase in air and ocean temperatures and raising of the sea level. Human activities are the main reason for this increase in the greenhouse gas concentrations and CO_2 is predominant.[1] Intergovernmental Panel on Climate Change (IPCC) has estimated a global temperature rise in the range of 1.1-6.4 K during this century.[2, 3] IPCC has recommended governments to implement policies to create incentives to further mitigate climate change.[1]

The current energy infrastructure is heavily dependent on fossil fuels as the main source of energy. Consumption of such fuels releases an estimate of 28 Gt CO_2/year to the atmosphere.[4] With no other alternative energy sources in near future, a continuous consumption of fossil fuels is expected during the 21st century and beyond. Therefore, any strategy for mitigation of the climate change has to account for a continued use of fossil fuels. Capture and sequestration of carbon dioxide CCS is a central strategy to many such strategies, as it offers the opportunity to meet an increasing demand for fossil fuel energy in short to medium term until alternative clean sources of energy are found.[5-8] CCS refers to capturing the carbon dioxide produced by combustion through a suite of technologies and subsequent compression and injection into the geological strata. Implementation of CCS includes probable financial cost and energy penalty to produce a pure stream of CO_2.[9] In existing technologies, carbon dioxide is captured either before combustion or after combustion of the fuel. A schematic illustration of the existing processes can be seen in Figure 1. Postcombustion capture methods are closest to the market since they can be adapted to the existing power plants without major reconstruction of the facilities. The precombustion and oxyfuel processes are projected to attain higher efficiencies for CO_2 capture, which will compensate for their extensive investments in longer term.[10]

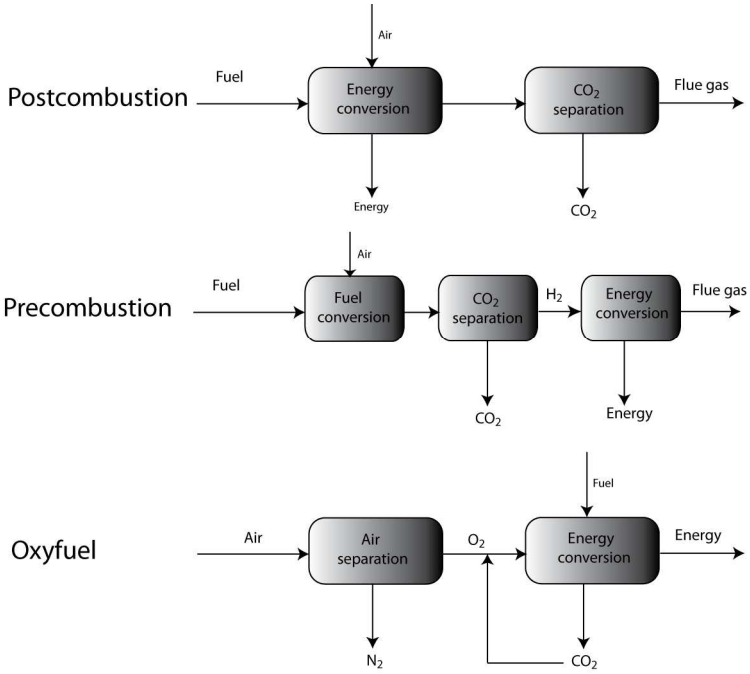

Figure 1 *Schematic illustration of existing processes for capturing carbon dioxide.*

Current technology for post-combustion capture involves wet-scrubbing of flue gases with amine-based sorbents.[5,11-13] The drawbacks associated with this technique is mainly manifested in the high cost of carbon capture and have driven researchers to find less expensive alternatives.[14-16] Solvent scrubbing with amines could in addition be coupled to potential environmental hazards.

Significant research have been dedicated, in particular, to overcoming the energy intensive solvent regeneration step and chemical degradation issues, which are characteristic of solvent based gas separation. The key element is to find new materials that can replace the solvents with similar or higher efficiency at a lower cost. Examples of new materials include physical absorbents, adsorption on solids using pressure or temperature swing adsorption processes, cryogenic distillation, gas hydrate formation and chemical-looping combustion using metal oxides among others.[17,18]

Adsorbents

Solid physical adsorbents in particular have found great deal of attention due to their significant advantages for energy efficiency compared with absorption processes. A variety of solid physical microporous and mesoporous adsorbents such as activated carbon, carbon molecular sieves, zeolites and chemically modified mesoporous material among others are considered for carbon capture.[14] The crucial element for physical adsorbents is the balance between the strong affinity for removing CO_2 from the gas mixture and the energy consumption required for their regeneration. An optimal physical adsorbent should possess high adsorption capacity, high selectivity and require low energy of regeneration. In addition the adsorbents should be thermally and mechanically stable and also time efficient to be used in many cycles. These rather conflicting properties require careful design of new materials.

One potential candidate is chemically modified mesoporous silica. The rather large pores, facilitating rapid mass transport, together with high adsorption capacity and increased selectivity due to chemical modification makes these materials interesting in gas separation. Amine modified silica adsorbents, being one of the potential alternatives, falls into this category of adsorbents. They have been developed in analogy to the existing CO_2 scrubbing with amine solutions.[17] However, a complete understanding of the chemistry involved and optimization of these adsorbents to satisfy the demands are still a matter of discussion and needs to be investigated. In this thesis amine-modified silica was studied to answer some of the questions related to the CO_2 separation.

Another route to capture carbon dioxide is employing the reversible reaction between calcium oxide and carbon dioxide to form calcium carbonate.[19-21] A schematic illustration of this process can be seen in Figure 2. In fact the post-combustion carbonate cycle has been chosen as one of the two highest priorities for future research and development by the Technology Task Force of the European Technology Platform for Zero Emission Power Plants.[22]

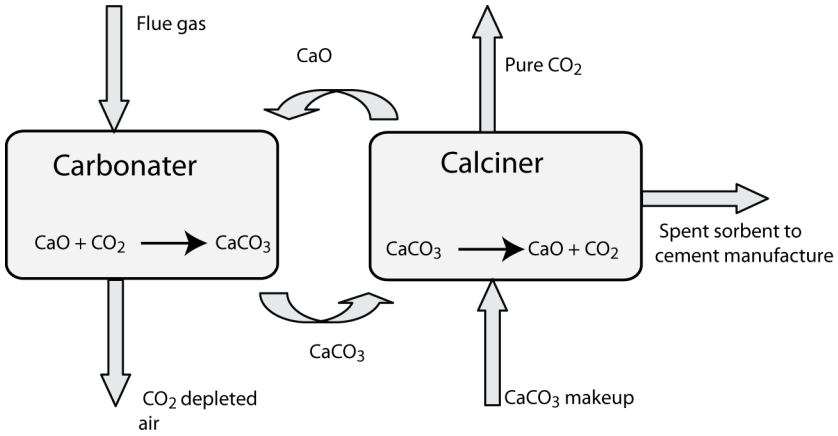

Figure 2 *Post-combustion carbon dioxide capture by calcination and carbonation route.*

The drawback of this technique is mainly the short life time of the calcium oxide as the absorber. This problem is related to the particle growth and increased diffusion time with increasing the cycles of calcination and carbonation which reduces the life time of these absorbents.[22] The main source of calcium oxide is the natural calcium carbonate or limestone. Using synthetic calcium carbonate as the calcium oxide source, has shown to be more advantagous.[24-27] In particular, nano-sized calcium carbonate showed promising properties to be used as carbon dioxide absorbent.[28] Understanding crystallization of calcium carbonate might help to design new processes and efficient absorbents.

In this thesis, I present the optimization of amine modified silica and investigation of the chemistry of CO_2 adsorption on these materials under different circumstances. Three papers in this thesis focused on such CO_2 adsorbents. In the second part, the crystallization pathway of calcium carbonate and effects of different experimental conditions are going to be presented through two other papers. Carbon dioxide absorption with these calcium carbonates is not presented, but could be a natural extension of this thesis.

References

(1) IPCC, Climate change 2007: synthesis report. Contribution of Working Groups I, II, and III to the forth assessment report of the intergovernmental panel on climate change. In Pachauri KP, Reisinger A, editors. IPCC: Geneva, Switzerland; 2007.

(2) IPCC, Intergovernmental panel on climate change special report on emissions scenarios. Nakicenovic N, Swart R, editors. IPCC: Geneva, Switzerland; 2000.

(3) IPCC. Climate change 2001: synthesis report. Contribution of Working Groups I, II, and III to the forth assessment report of the intergovernmental panel on climate change. In: Watson RT, editor. IPCC: Cambridge, UK; 2001.

(4) IEA. World energy outlook, 2008. Paris, France: IEA; 2008.

(5) Gibbins, J.; Chalmers, H. *Energy Policy* **2008**, *36*, 4317–4322.

(6) Burton, J. J. *Chem. Eng. News* **2008**, *86*, 5–6.

(7) Herzog, H.; Eliasson, B.; Kaarstad, O. *Sci.Am.* **2000**, *282*, 72–79.

(8) Aaron, D.; Tsouris, C. *Sep. Sci. Technol.* **2005**, *40*, 321–348.

(9) Abanades, J. C.; Rubin, E. S.; Anthony, E. J. *Ind. Eng. Chem. Res.* **2004**, *43*, 3462–3466.

(10) IPCC, *IPCC Special Report on Carbon Dioxide Capture and Storage*, Cambridge University Press, Cambridge, **2005**.

(11) Rochelle, G. T. *Science* **2009**, *325*, 1652–1654.

(12) Pellegrini, L. A.; Moioli, S.; Gamba, S. *Chem. Eng. Res. Des.* **2011**, *89*, 1676–1683.

(13) Padurean, A.; Cormos, C.-C.; Cormos, A.-M.; Agachi, P.-S. *Int. J. Greenh. Gas Control* **2011**, *5*, 676–685.

(14) Choi, S.; Drese, J. H.; Jones, C. W. *Chemsuschem* **2009**, *2*, 796–854.

(15) Hedin, N.; Chen, L.; Laaksonen, A. *Nanoscale* **2010**, *2*, 1819–1841.

(16) Chaffee, A. L.; Knowles, G. P.; Liang, Z.; Zhany, J.; Xiao, P.; Webley, P. A. *Int. J. Greenh. Gas Control* **2007**, *1*, 11–18.

(17) D'Alessandro, D. M.; Smit, B.; Long, J. R. *Angew. Chem.Int. Ed.* **2010**, *49*, 6058–6082.

(18) Yang, H.; Xu, Z.; Fan, M.; Gupta, R.; Slimane, R. B.; Bland, A. E.; Wright, I. *J. Environ. Sci.* **2008**, *20*, 14–27.

(19) Blamey, J.; Anthony, E. J.; Wang, J.; Fennell, P. S. *Prog. Energy Combust. Sci.* **2010**, *36*, 260–279.

(20) Yu, F.-C.; Phalak, N.; Sun, Z.; Fan, L.-S. *Ind. Eng. Chem. Res.* **2012**, *51*, 2133–2142.

(21) Alonso, M.; Rodriguez, N.; Gonzalez, B.; Grasa, G.; Murillo, R.; Abanades, J. C. *Int. J. Greenh. Gas Control* **2010**, *4*, 167–173.

(22) The EU technology platform for zero emission fossil fuel power plants, recommendations for RTD, support actions and international collaboration

activities within FP7 energy workprogrammes in support of deployment of CCS in Europe, http://www.zeroemissionpltaform.eu/website/docs/ETP%20ZEP/TTech%20Input%20FP7%203rd%20call%20080418.pdf; 18 april 2008.
(23) Abanades, J. C.; Alvarez, D. *Energy Fuels* **2003**, *17*, 308–315.
(24) Gupta, H.; Fan, L.-S. *Ind. Eng. Chem. Res.* **2002**, *41*, 4035–4042.
(25) Li, Z.; Cai, N.; Huang, Y.; Han, H. *Energy Fuels* **2005**, *19*, 1447–1452.
(26) Pacciani, R.; Müller, C. R.; Davidson, J. F.; Dennis, J. S.; Hayhurst, A. N. *The Canadian Journal of Chemical Engineering* **2008**, *86*, 356–366.
(27) Dennis, J. S.; Pacciani, R. *Chem. Eng. Sci.* **2009**, *64*, 2147–2157.
(28) Florin, N. H.; Harris, A. T. *Chem. Eng. Sci.* **2009**, *64*, 187–191.

Chapter 1

Amine- modified silica

1.1 Introduction

Silicon dioxide or silica, originating from the latin word Silex, is found in nature as sand, quartz and in the wall cell of diatoms. The diversity of the forms of silica has made it possible to use this compound in a large range of applications. Porous silica, in particular, has found a great deal of interest in many scientific and industrial applications due to its excellent properties; high mechanical and thermal stability and a large specific surface area. The possibility to combine the properties of organic and inorganic building blocks within a single material is one of the most interesting features of silica. A thermally stable and robust inorganic substrate onto which a broad variety of organic molecules can be attached has meant it is used in many applications. Such applications are found in chromatography, catalysis, enzyme immobilization, sustained drug delivery, as adsorbents and environmental applications.[1–11] In this thesis the ability for silica to be organically modified with amine groups will be used to prepare adsorbents which can be used as CO_2 uptake agents. There are two main ways of altering the surface functionality of the porous silica surface. Here I describe the two methods briefly.[12]

1.1.1 Post-synthetic functionalization of silicas (grafting)

Post-synthetic functionalization refers to subsequent modification of the inner surface of the porous silica with organic groups. Organosilanes of the type $(R'O)_3SiR$ or less frequently chlorosilanes $ClSiR_3$ or silazanes $HN(SiR_3)_2$ react with the silanol (SiOH) groups on the silica surface, see Figure 1.1. This method of modification has several advantages. First, a large variety of functional groups can be used. Second, the porous structure of the silica substrate is typically preserved. The disadvantage

of post-synthetic modification would be the lack of homogeneity of the modified surfaces.

Figure 1.1 *Grafting (post-synthetic functionalization) for organic modification of porous pure silica with terminal organosilanes $(R´O)_3SiR$, R is the functional group.*

If the organosilanes react preferentially at the pore opening during the initial stages of the synthetic process, then the diffusion of further molecules into the centre of the pores can be impaired and the result will be a nonhomogenous distribution of the functional groups across the surface. Another disadvantage is reduction in the pore volume and surface area, which usually depends on the size of the organosilane molecule.

1.1.2 Co-condensation (direct synthesis)

Using co-condensation modification, a porous silica substrate is synthesized by co-condensing tetra-alkoxysilanes $(RO)_4Si$ (TEOS or TMOS) with terminal trialkoxyorganosilanes of the type $(R´O)_3SiR$. This method leads to materials with organic functional groups anchored covalently to the pore walls, see Figure 1.2.

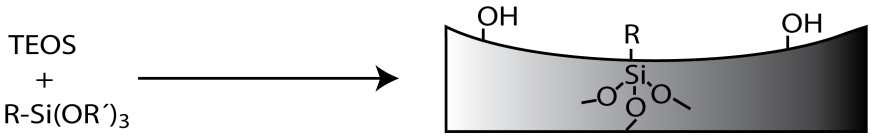

Figure 1.2 *Co-condensation method (direct synthesis) for the organic modification of porous functionalized silica, R is the functional group.*

Advantages of co-condensation are the homogenous distribution of the functional groups, and that pore blockage and reduction of the porosity are avoided. However, the method has several disadvantages. When

crystallizing mesoporous silica, silica with pore size 2-50 nm, the order decreases with increased concentration of $(R'O)_3SiR$. The proportion of terminal organics incorporated in the pore-wall is generally lower than what would correspond with the initial concentration of the reaction mixture. Homocondensation originating from the difference of the rate of hydrolysis and condensation of the different type of the silica precursors is an additional problem of co-condensation. The $(R'O)_3SiR$ tends to crosslink which each other and as a result the homogenous distribution of the functional groups are disturbed. These problems, together with that silica substrates synthesized by co-condensation cannot be calcined, and as a result less mechanical stability limit this method significantly.

In this thesis, the post-synthetic modification was used to modify the silica surface by propyl amine groups in order to make adsorbents for CO_2 adsorption.

1.1.3 Amine modified silica as CO_2 adsorbents.

Currently post-combustion CO_2 capture involves scrubbing the flue gases by liquid amines or alkanolamine solutions. This effective method suffers from several drawbacks, such as high energy consumption for regeneration of the liquids, corrosion of equipment, and environmental hazards due to leaking of these corrosive amines.[13] Efforts have been made to find economically beneficial alternatives of carbon capture which avoids these problems. Significant attention is currently given to the adsorption driven separation of CO_2 from N_2 rich flue gases. Recent simulations indicate that solid substrates with lower heat capacity compared to the liquid solutions and with high selectivity for CO_2 are promising to reduce the cost for CO_2 capture significantly.[14,15] Amine modified sorbents have been shown to be one the promising candidates for CO_2-over-N_2 selection.[16–18] These sorbents have been designed in analogy to the liquid amine CO_2 scrubbing solvents. Mesoporous silica in particular has found a great deal of attention due to properties like high surface area and large enough pores to facilitate the mass transport. Much work has been devoted to modified silica with ordered pore structure such as MCM41, SBA-15 and others as their detailed pore structures have been well characterized.[19,20] However, Goeppert et al.

suggested that much simpler substrates, such as fumed or precipitated silica, could not only be less expensive, but also, in some aspects, be better CO_2 sorbents, when being modified with amine groups.[11] In the majority of the cases post-synthetic modification has been used to modify these adsorbents, but simple coating and filling of the pores have also been used. A large number of studies have investigated the silica substrates modified chemically by n-propylamine functional groups.[17,21–28] They have shown that these sorbents adsorbed significant amounts of CO_2 by chemisorption. Angeletti et al showed that propylamine modified silica have excellent sites for Knoevenagel condensation.[28] In a number of studies mesoporous silica has been modified with amine functional groups other than propylamine.[18,24,29–34] Kim et al observed that the silicas modified with n-propylamine adsorb more CO_2 in comparison to silicas modified with polymeric propylamine, pyrrolidinepropyl and polyethylenimine.[24] However, there are reports that pore expanded MCM-41 modified with triamine groups adsorbed significant amount of CO_2 in which they outperformed adsorbents with high CO_2 adsorption capacity like zeolite X.[29–32] In most of these studies a simple procedure of post-synthetic modification have been used without optimization of the synthetic conditions. Usually without taking into consideration of how the synthetic condition reflect on the performance of the adsorbents. In this thesis, n-propylamine was used as the modifying agent and the synthetic conditions were studied in detail. Amine modified silica with different content of amine groups was obtained and allowed detailed studies of the CO_2 adsorption chemistry.

1.1.4 The chemistry of CO_2 adsorption on amine modified silica

The reaction chemistry of the CO_2-amine in liquid systems is largely known.[35–40] The main product of the reaction between CO_2 and primary amines is the ammonium-carbamate ion pairs, but formation of carbamic acid, and bicarbonates (in aqueous solutions) are also observed, see Figure 1.3. It appears that various types of compounds, depending on the polarity of the solvent, are formed. Carbamate species form in protophobic solvents while carbamic acid is stabilized through hydrogen bonding in protophilic solvents.[41] In aqueous solutions carbamates react

further and form bicarbonates. These compounds are thermally instable and the solution can be regenerated by heating. The main cost of the CO_2 capture by liquid amines also lies in the regeneration of the solution.

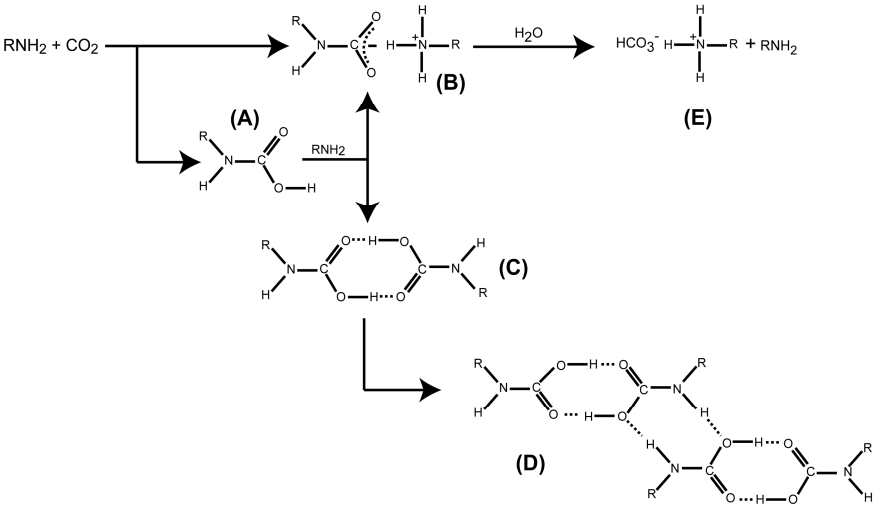

Figure 1.3 *Reactions occurring during the CO_2 absorption in amine liquid solutions and the formed species. (A) Carbamic acid, (B) alkyammonium carbamate ion pair, (C) dimeric carbamic acid, (D) tetrameric carbamic acid and (E) bicarbonate formation.*

The lower heat capacity of the amine modified solid adsorbents combined with high selectivity could potentially reduce the cost for CO_2 capture.[15]

The CO_2-amine chemistry in tethered amine modified adsorbents although similar but shows some differences to that of liquid amines. The translational diffusion of the amines is absent for tethered amine groups. Therefore, the chemistry of CO_2-amine on the amine modified sorbents is expected to be somehow different. The detailed CO_2-amine chemistry is under investigation.[14,42–45] Formation of alkylammonium alkylcarbamate salts has been observed upon the reaction of the CO_2 and tethered amine groups. The ammonium carbamate ion pairs require two amine groups to be close to each other. Hence, the importance of distribution of the amine groups by the choice of the modification route becomes crucial in the

formation of carbamates.[46] Another compound that can form is the carbamic acid. In liquid state this compound is stable in protophilic solvents, which provide hydrogen bonding into dimeric and tetrameric forms. The formation of the tetrameric and possibly dimeric carbamic acids can be excluded in the amine modified solids. Thermodynamically unstable carbamic acid is then believed to be stabilized through hydrogen bonding with silanol groups or adjacent NH_2 groups. There is also the possibility of the esterification of the carbamic acid together with the silanol groups to form silylalkylcarbamates.[47] This reaction requires dry conditions since the presence of water causes hydrolysis of silylalkylcarbamate. Humid gas mixture usually causes an enhancement of the uptake of CO_2 on amine modified silicas. This enhancement was speculated to relate to the formation of bicarbonates and usually in the absent of spectroscopical evidence.[31,46,48–50] Recent studies seems to exclude any formation of the bicarbonates.[43,47] The enhancement of the CO_2 uptake is then attributed to other formed species. This feature is one of the questions that are addressed in this thesis.

1.2 Experimental

1.2.1 Materials and syntheses

Substrate:

Davisil™ LC60 (Grace Davison, US), an amorphous silica material with a high specific surface area, was used as the substrate (paper I, II and III). The substrate had an average particle size of 40–63 µm and a surface area of 550 m^2/g. The irregular morphology of these particles can be seen in Figure 1.4.

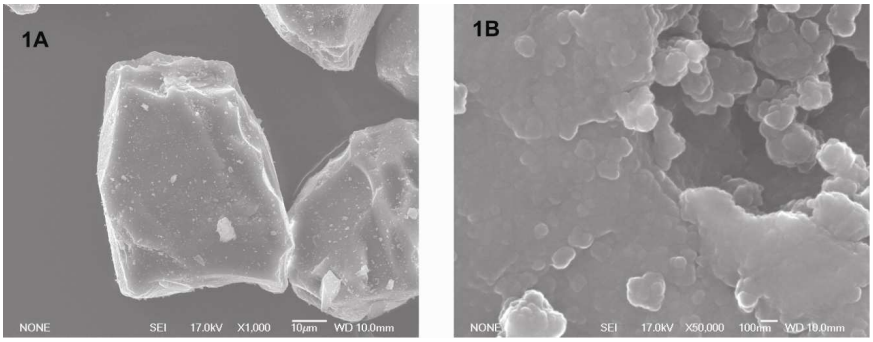

Figure 1.4 *SEM micrographs showing the irregular shapes of DavisilTM with particle sizes of 40-63 µm used as the substrate in post-synthetic modification.*

Modifying agent:

Three different types of organosilanes were mainly used in the modification of Davisil™, see Figure 1.5.

a) Aminopropyltriethoxysilane (APTES) [CAS: 919-30-2] Sigma Aldrich 99%) (paper I, II and III)

b) Propyl-bis(2-hydroxyethy)amine(BHEAP) paper (II)

c) propyl-N, N-dimethylacetamidine (DAMP) paper(II)

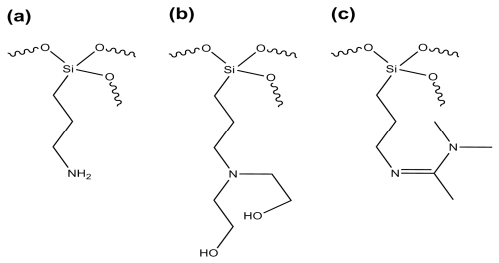

Figure 1.5 *modification agents a) n-propylamine triethoxysilane (APTES), b) Propyl-bis(2-hydroxyethy)amine (BHEAP) and c)propyl-N, N-dimethylacetadimine.*

1.2.2 Post-synthetic modification with propylamine groups

Post-synthetic modification of the silica substrate was carried out in toluene under flow of N_2. Substrates were used as received and with various pre-treatments: acid treatment with 2 mol/dm^3 HCl at 60 °C overnight, or degassing at a temperature of 400 °C at very low pressure overnight. Detailed description of the experimental conditions can be found in paper I and II. APTES was used in modification of Davisil™ in 22 different samples, 19 of the samples were included in the systematic studies using fractional factorial design, see paper I for details. The conditions for the modification of the other three samples are found in paper II.

1.2.3 Characterizations and methods

1.2.3.1 Experimental design and analysis of variance

Experiments conducted in paper I were randomized and analyzed by computer software MODDE™. A fractional factorial design 2_V^{5-1} was chosen to analyze the effect of the experimental conditions. The content of nitrogen, corresponding to the content of amine groups and the uptake of CO_2 at 25 °C and 760 Torr of CO_2 were used as the responses to the experimental design.

1.2.3.2 Nuclear magnetic resonance (NMR) spectroscopy

Direct polarization experiments were used to record ^{29}Si and ^{1}H NMR spectra on a Chemagnetics Infinity 400 spectrometer operating at 79.49, and 400.16 MHz, for ^{29}Si, and ^{1}H respectively. Magic angle spinning (MAS) conditions of 8.00 kHz were used in a double resonance 6 mm probe head acquiring ^{29}Si NMR spectra. A MAS rate of 18.0 kHz were used in a double resonance 3.2 mm probe head acquiring ^{1}H NMR spectra. Detail conditions of the measurement can be found in paper I.

1.2.3.3 Fourier transform infrared spectroscopy (FTIR)

FTIR spectroscopic measurements were carried out on a Varian 670-IR spectrometer equipped with a transmission cell and vacuum system constructed in-house[44,47], and a mercury telluride (MCT) detector, see Figure 1.6. Self supporting pellets were made from 25-30 mg of the samples. Details of the measurements are presented in paper III. Briefly, a single beam spectrum was recorded for the empty cell under vacuum condition as the background for absorbance spectra of the samples recorded under dynamic vacuum condition. These spectra were used as the background for the spectra of samples contacted with a CO_2 containing atmosphere. Hence, these spectra corresponded only to changes related to CO_2 adsorption. Spectra along the adsorption branch were recorded by successively increasing the pressure of CO_2 from 1 to 760 Torr. Contributions from gaseous CO_2 to the IR spectra were compensated for by recording the corresponding gaseous CO_2 spectra in the cell at all studied pressures of CO_2 and subtracting it from the original spectra. The Si-O-Si overtone bands at 1860 and 2000 cm^{-1} were used as internal standards to compensate for differences in the pellet thickness among different samples.

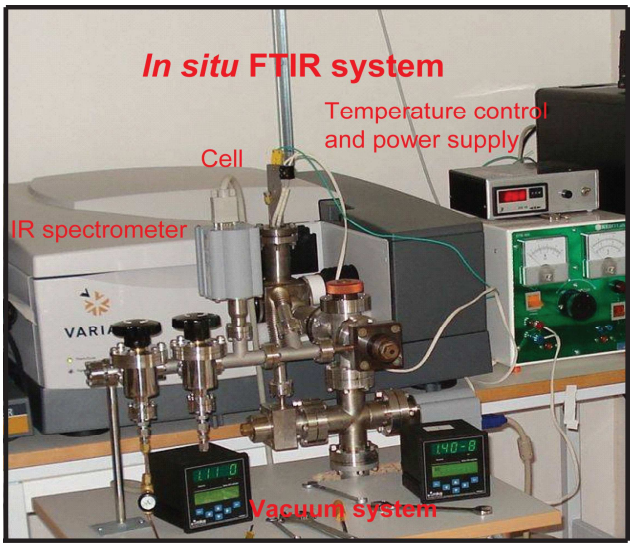

Figure 1.6 *The homebuilt adsorption cell and in house assembled vacuum system connected to a Varian 670- IR spectrometer.*

1.2.3.4 Gas adsorption measurements

Nitrogen and CO_2 adsorption were measured using a Micromeritics ASAP2020 device or a Micromeritics Gemini™ 2375 device. A detailed description of the measurements can be found in paper I, II and III. A schematic presentation of the temperature controlled adsorption measurements can be seen in Figure 1.7. All samples were degassed under, vacuum or flow of dry nitrogen at elevated temperatures before adsorption, see paper I and II. CO_2 adsorption measurements were conducted at the pressure range 1-760 Torr. The humid CO_2 was achieved by purging the pure gas through liquid water in sealed bottle containing 2 dm^3 water and allowing it to saturate overnight, for details see paper I, II.

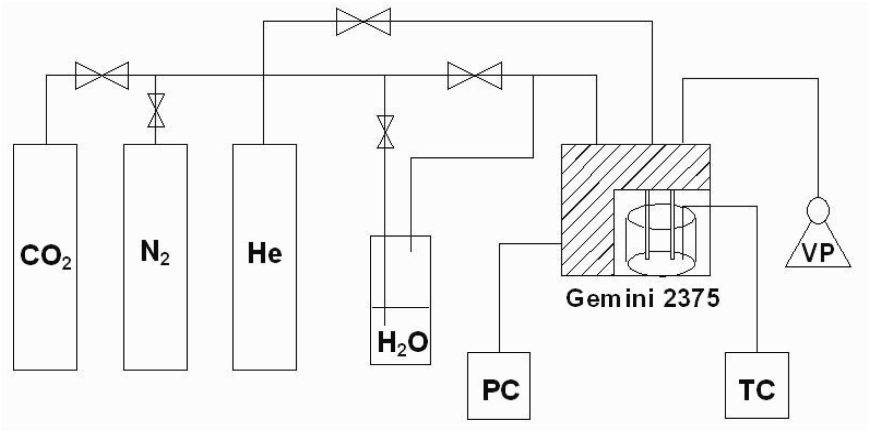

Figure 1.7 *Schematic presentation of the volumetric adsorption on Micrometrics Gemini™ 2375 used to measure temperature and pressure dependent uptake of CO_2 and N_2. The humid conditions were reached by purging the gas through liquid H_2O. PC, pressure controller, TC temperature controller and VP vacuum pump.*

1.2.3.5 Quantifications of n-propylamine moieties

The content of C and N corresponding to the content of amine groups was determined by elemental analysis. Thermogravimetric analysis (TGA) was used to record the mass loss on heating, using a Perkin Elmer TAG7 instrument in dry air. Samples were heated from 50 °C to 950 °C at a rate of 10 °C/min in a platinum cup.

1.2.3.6 Scanning electron microscopy (SEM)

A JEOL JSM-7000F microscope operating at 15 kV with a working distance of 10 mm was used to record images of the Davisl™ substrates sprinkled on Oxford Aluminum stubs coated by dried colloidal carbon.

1.3 Results and discussion

Results related to characterization of the amine-modifed material are discussed. A short description of the characterization and methods will be presented. In addition, results from fractional factorial design and uptake and chemistry of CO_2 on amine modified silicas are discussed.

1.3.1 ^{29}Si- solid state NMR

Nuclear Magnetic Resonance NMR is one of the most important techniques to study the structure and dynamics of various compounds. Solid state NMR spectroscopy in particular has been shown to be very useful in studying the molecular details of the interfaces in mesoporous materials.[51–53] The basic principle of this technique is that some nuclei possess an intrinsic property called spin and with it a spin angular momentum and a magnetic moment. This property can be imagined as if the nuclei act as a small magnet. Without going too much into the details, if a strong external magnetic field is applied on the nuclei with spin angular momentum, the randomly oriented spins are going to partially align along the external field. These partially aligned spins precess in a classical description around the applied field. The frequency of the precssion, called Larmor frequency, depends on the type of nuclei, the applied filed strength and to a small extent on local interactions. Applying another field within the radio frequency (rf) can change the orientation of the net magnetic moment. When this rf filed is removed, the net magnetic moment will precess along the external field and induces a current in the coil with which the rf pulse was applied. This signal is called the NMR signal and the process by which the net magnetic moment restores the equilibrium state is called relaxation. Useful information can be obtained from the interactions of the spin with its surrounding. These interactions are the chemical shift (originating from the movement of the electrons surrounding the nuclei), dipolar coupling, J-coupling and quadrupolar coupling. The effect of these

interactions will be reflected in the magnetic moment of the spins and hence in the precession frequency.

1.3.1.1 Magic angle spinning

In solid state NMR the NMR signal is affected by both isotropic and anisotropic parts of the interactions. For this reason the peaks in SSNMR are usually broad. The idea of magic angle spinning is that many interactions relevant for NMR depends on the angle by which the sample is oriented with respect to the applied filed. The line broadening due to chemical shift anisotropy is then eliminated by spinning the sample at high frequencies at the angle 54.74°, called magic angle. This angle relates to the root of the second order Legendre polynomial $x=\arccos(1/\sqrt{3})$. Higher resolution peaks are obtained by increasing the spinning frequency.

1.3.1.2 ^{29}Si SS-NMR of silica and amine modified silica

Silica consists mainly of tetrahedrally coordinated silicones covalently bounded with oxygens. The ^{29}Si NMR signal is very sensitive to the connectivity of the SiO_4 units. Figure 1.8 shows an illustration of how the connectivity of the SiO_4 units affects the chemical shift. A fully condensed SiO_4 unit, SiO_4 unit covalently connected to four other SiO_4 units, has a chemical shift in the range (-120)-(-100) ppm and the signal is denoted by Q_4. However, not all the units are fully condensed in a silica sample and there is a lack of connectivity in these materials. In pure silica one or more Si atoms is then replaced by a hydrogen atom. Lack of connectivity is then reflected in the chemical shift. The chemical shift changes by ~10 ppm for each change from Q_4 to Q_3 and from Q_2 to Q_1 and so on. In an propylamine modified silica there are Si atoms which are connected to the hydrocarbon chain of the propylamine groups. ^{29}Si NMR provides a good mean by which different grafted groups can be detected. Figure 1.8 shows some of these groups and the corresponding chemical shift. A T_3 signal at -67 ppm emerged from ^{29}Si nuclei which are connected to a carbon atom and to three bridging oxygens. T_2 signal at ~-59 ppm comes from ^{29}Si nuclei which are connected to one carbon atom and to two bridging oxygen and one silanol group. In the same way T_1 signal at ~-50

ppm comes from ^{29}Si nuclei connected to a carbon atom and to one bridging oxygen and two silanol groups.[54–56]

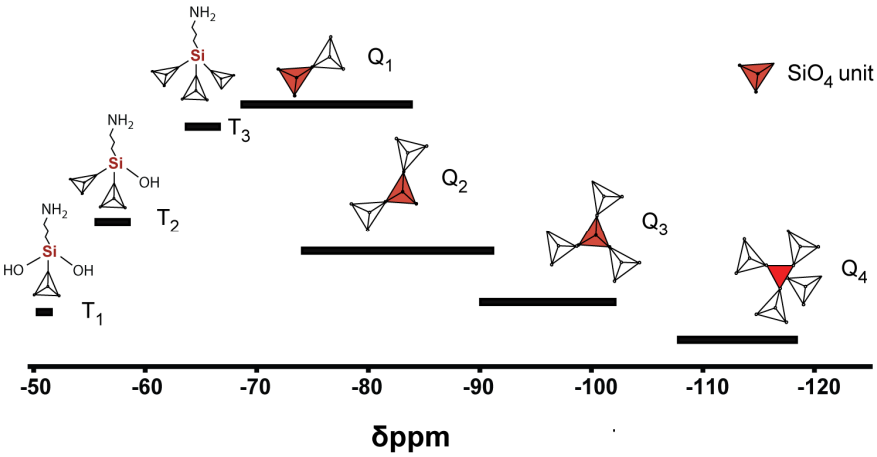

Figure 1.8 *An illustration about the different connectivity of the Si nuclei in propyl-amine modified silica and the corresponding chemical shift values in ^{29}Si NMR.*

In a perfect homogenous and fully coated surface we would expect to see T_3 signals together with the Q_n signals from the bulk material. Figure 1.9 shows a direct polarization ^{29}Si NMR spectrum of the amine modified silica (PA20), the sample with the largest amount of n-propylamine groups. This spectrum shows peaks corresponding to Q_4 and Q_3. Existence of Q_3 signal indicates that all the Q_3 (Si-OH) sites were not available to the reaction with APTES. The T_3 and T_2 groups are represented by the peaks at -68 ppm and -60 ppm. The existence of T_2 signals means that the surface has a heterogeneous distribution of the functional groups. The fraction of the fully condensed APTES on silica can be expressed in the ratio $T_3/(T_2+T_3)$ and was about 70% for sample PA20. This ratio is expected to be lower for other amine modified silica. Note that these experiments were very time consuming and could be applied only to samples with high content amine groups. A high content of T_3 signals suggest that amine groups have at least the proximity needed to form the ammonium carbamate groups and the material in question will show a high chemisorption of CO_2.

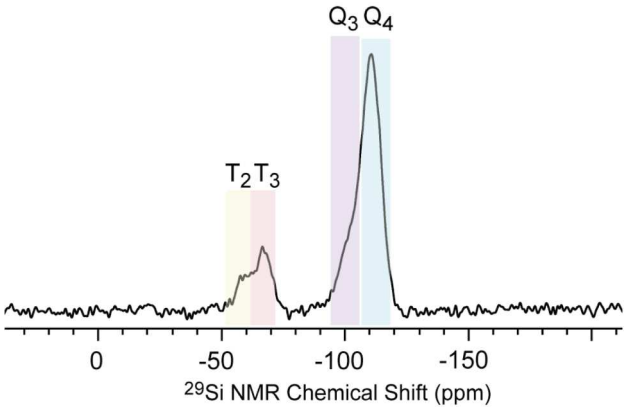

Figure 1.9 *Magic-angle spinning solid state 29Si NMR spectra of Davisil modified with (3-aminopropyltriethoxysilane) APTES.*

1.3.2 FTIR spectroscopy of the silica and amine modified silica

Infrared spectroscopy is based on vibrations of the atoms in molecule of a solid. The key feature for any molecule to show infrared absorption is the change in electric dipole moment of the molecule during vibration. For this reason, homonuclear species such as N_2 are IR inactive since no net change in the dipole moment occurs during the vibration of its bond. The IR absorption then excites the vibration from its ground state to higher vibrational states. The energy difference between two vibration states can be explained by following equation for the harmonic oscillation.

$$\Delta E = h\nu_m = \frac{h}{2\pi}\sqrt{\frac{k}{\mu}}$$

In which υ_m is the vibration frequency, h is the Planck's constant, k is the force constant, corresponding to the strength of a bond, and μ is the reduced mass. It is important to stress that the vibrations in real molecules are not harmonic oscillation because of effects such as Columbic repulsion, and in interatomic distances that approach bond dissociation. Still, this equation describes the dependency of the vibrational frequency on the bond strength rather well. Interactions such

as hydrogen bonding results in the weakening of the bond, *k* will be affected, and that changes the vibrational frequency. This effect is very well presented in the vibrational frequency of the OH groups on silica surface. Based on these differences, silanol groups are divided into four groups; isolated or free silanol, geminal silanols, vicinal or hydrogen bonded OH groups and internal Si-OH groups. A schematic illustration can be seen in figure 1.10.

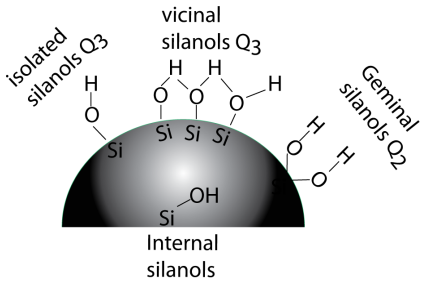

Figure 1.10 *Different types of silanol groups on the surface of porous silica and corresponding Qn terminology used in SS ^{29}Si NMR.*

Silanols absorb IR radiation in the broad region of 3800-3000 cm^{-1}.[57] Usually a sharp band at about 3730-3750 cm^{-1} accompanied by a broad absorption in the range 3600-3000 cm^{-1} can be seen in the spectra of silica, see figure 1.11a. The sharp band has been assigned to the isolated or geminal silanols. The effect of hydrogen bonding can be seen in the lowering of the vibrational frequency of the vicinal silanols. The hydrogen bonds between the hydrogen of a silanol group with adjacent water of OH groups can be of different strength; hence the vibrational frequency will also vary. As a result we see a broad absorption band in the range of 3600-3000 cm^{-1}. The silanol groups act as anchors for the functionalization of silica surface. One way to observe the changes on the silica surface upon modification with amine groups is the changes of the silanol groups. The spectrum of APTES modified silica is shown in Figure 1.11b. The changes that can be seen is the complete disappearance of the isolated or geminal OH groups indicating that these groups have reacted or involved in hydrogen bonding. Existence of a broad band at the range 3600-3500 cm^{-1} suggests that the remaining OH groups on the surface probably are vicinal and internal silanol groups.

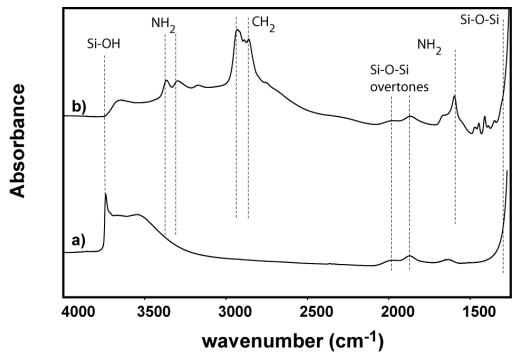

Figure 1.11 *IR spectra of under vacuum conditions of a) pure porous amorphous silica (Davisil) and b) APTES (3-amiopropyltriethoxysilane) modifed silica (sample PA20).*

This result confirms finding from ^{29}Si NMR in which Q_3 signals could be detected. IR spectroscopy also reveals the existence of new species after modification of the surface. There are bands at 3373 and 3309 cm^{-1} corresponding to asymmetric and symmetric stretching modes of NH_2 groups and two bands at 2930 and 2869 cm^{-1} corresponding to the aliphatic CH stretching region. These bands confirm that the functionalization of the surface with APTES has been successful. However, no information about the distribution and conformation of the functional groups can be extracted form IR spectra.

1.3.3 Experimental design and fractional factorial design

The purpose of conducting experiments is usually to either confirm or reject a hypothesis that has been made based on the previous knowledge. The outcome of the new experiments will eventually result in an increased knowledge and this is the foundation of the scientific approach to answer the questions in our universe. A self-evident statement would be to say that the results of an experiment will be dependent on the studied variables of that experiment which simply can be stated as a mathematical equation.

$$Result = f(experimental\ variables)$$

However, what we know from the complexity of nature is that these functions are seldom known and to find an approximation is the best we can do. An appropriate approximation is by Taylor expansion.

$$y = f(0) + \sum_{i=1}^{k} \frac{\partial f(0)}{\partial x_i} \cdot x_i + \sum_{i=1}^{k} \sum_{j=1}^{k} \frac{\partial f(0)}{\partial x_i \cdot \partial x_j} \cdot x_j \cdot x_i + R(x) + e$$

Which can then be simply written as:

$$y = \beta_0 + \beta_1 x_1 + \beta_2 x_2 + ...\beta_k x_k + \beta_{ij} x_i . x_j .... + \beta_{ii} x_i^2 + ..R(x) + e$$

The coefficients β in the polynomial model is called the parameters of the model. Values of these parameters denote the importance of each variable on the response or the results. These parameters are usually estimated by multiple linear regressions in which the composite sum of the squared deviations in between polynomial model and experimental results is minimized. In an adequate model the residuals, the difference between observed and calculated results, should not be greater than the experimental error. The evaluation of the estimated model can then be confirmed by means of statistical analysis of the error.

1.3.3.1 Error analysis

Validation of a model is based on how well they can predict the experimental results in the experimental domain. This means that the difference between the calculated and observed results should only reflect the random experimental errors. There are a number of tests that can be performed to examine the validation of a model. Here we mention some briefly.

1.3.3.2 Analysis of variance (ANOVA)

This analysis is based on the random distribution of the experimental errors. We have a number of terms in this analysis, which we present in Table 1.

Table 1 *The analysis of variance table*

Source of variation	Degrees of freedom	Sum of squrares(SS)	Mean square (MS)	F ratio
Total	n	$\sum_i y_i^2$		
Corrected for the mean	$n-1$	$\sum_i^n y_i^2 - \frac{1}{n}(\sum y_i^2)$	$\frac{\sum_i^n y_i^2 - \frac{1}{n}(\sum y_i^2)}{n-1}$	
Corrected due to regression	p	$\sum_i^n y_{i,calc}^2$	$MSR = \frac{\sum_i^n y_{i,calc}^2}{p}$	$\frac{MSR}{MSE}$
Residuals	$n-p$	$\sum_{i=1}^N (y_{i,calc} - y_i)^2 = \sum_{i=1}^N e_i^2$	$MSE = \frac{\sum_{i=1}^N e_i^2}{n-p}$	
Lack of fit	$n-p-\sum_k n_k - 1$	$\sum_{i=1}^N e_i^2 - \sum_i s_i^2$	$\frac{\sum_{i=1}^N e_i^2 - \sum_i s_i^2}{n-p-\sum_k n_k - 1}$	$\frac{MSE}{\sum_i s_i^2}$
Pure error	$\sum_k n_k - 1$	$\sum_{i=1}^k (y_{i,calc} - y_i)^2 = \sum_i s_i^2$	$\frac{\sum_i s_i^2}{\sum_k n_k - 1}$	

Analysis of variance table provide us with two tests. The goodness of regression is tested by obtaining the ratio between sum of mean squares due to regression (*MSR)* and sum of mean square due to residual (*MSE)*. For an adequate regression, this ratio should be larger than the critical F ratio for *p* and *n-p* degrees of freedom. The second test is the lack of fit. In this test the ratio between *MSE* and mean sum of squares due to pure error s_i^2 is obtained providing that there is another independent estimation of the variance s_i^2 . The model does not have a lack of fit if this ratio is less than the critical F ratio value for *n-p*, and n_k*-1*.

1.3.3.3 Residuals

ANOVA provides us with the information about the validity of the model and the significance of the variables on the estimated model. However, for the ANOVA to give correct description of the model, systematic errors should not exist. Analyzing the residuals is one way to make sure about the lack of systematic error. The following plots can be made to recognize existence of systematic errors.

Normal probability plot of residuals

In this plot the normal probability are plotted versus residuals. If the residuals are random, then they should show a normal distribution. The plot will then show a straight line. If there is significant deviation from the straight line, we would expect that there is a systematic error in the system.

Plot of residuals versus predicted values

In this plot the residuals are plotted versus calculated values in each case. If the residuals increase as the predicted values increase, a log transformation of the response is required and the analysis should be done accordingly.

Plot of residuals versus run order

Results or responses obtained from experiments should be independent from external factors such as variation in room temperature or who performs the experiments. Randomization of the run order is one way of avoiding the influence of such external factors. In such a test the residuals are usually plotted against the run order. The existence of a pattern in this plot indicates that some systematic error has been transferred into the random errors and the analysis has to be done properly.

These statistical analyses are necessary to evaluate whether the function is appropriate to describe and predict the results in the experimental domain of the system. However, for the analysis to make sense the experiments have to be designed in way that they reflect the studied variables.

1.3.3.4 Fractional factorial design

The evaluation of the model needs careful design of experiments. In most experiments an exact estimation of the response surface model is not the objective, but we want to see the impact of the experimental variables on the results. As the number of these variables increase so does the number of experiments, time and resources required to run the experiments. One way of designing the experiments is by implementing the factorial design approach.[58–60] In this approach each variable is usually varied between

two levels, one low and one high. The number of experiments required is 2^k and dependent on the number of variables k. This design gives a complete evaluation of the linear and interaction dependencies of the variables, but as the number of variables increases the time and also resources that are needed becomes important. This problem is usually solved by using the fractional factorial design. This design reasonably assumes that the interaction effects between three or more variables are small compared to main or two-variable interaction effects. The fractional factorial design then reduces the number of experiments to 2^{k-p} in which p describes the size of the fraction of the full factorial design. The experiments are chosen in a way that they span the largest space that is spanned by the experimental domain, see Figure 1.12. For example in a three variable experimental domain a total number of eight experiments are needed to evaluate a full factorial design while in a fractional factorial design (1/2) only four experiments are needed.

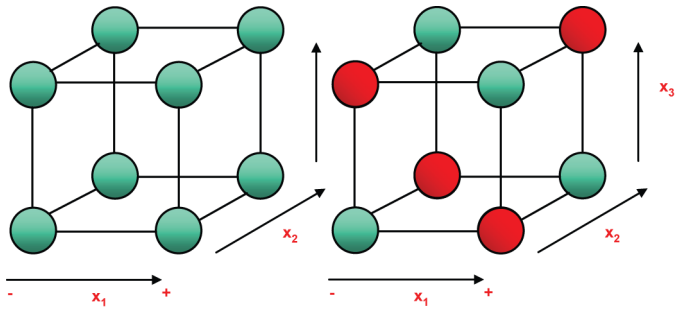

Figure 1.12 *Illustration of the used space in an experimental domain when full factorial design(left) is replaced by fractional factorial design (right).*

In this example the main effects are confounded with the two way-variable interactions. This means that the contribution of the interaction effects is included in the main effects but because of the small or negligible influence they will not affect the results. The resolution of a fractional factorial design is then defined by the way variables are confounded with the higher order of variable interactions, for example a resolution of V means that the main effects are confounded with the 4-way interactions and the two-way interactions are confounded with 3-way interaction effects. The analysis of the residuals will be employed to

see the validity of the model as mentioned before. Fractional factorial design offers a descent method for screening and identifying the most important parameters in chemical systems. In this study this approach has been selected to investigate the impact of some experimental variables on the functionalization of porous silica with amine moieties and the corresponding sensitivity for uptake of CO_2.

1.3.4 Fractional factorial design in modification of porous silica surface

We used a resolution V in the fractional factorial design, which confounded the main effects with four-variable interactions, and the two-way interactions with three variable interactions, details can be found in paper I.

The different conditions used, as well as the responses (Y_1 and Y_2) measured, are presented for APTES modified Davisil™ in a matrix form in Table 2. I will briefly present the most important results from this study.

Table 2 *Fractional Factorial experimental design for APTES modified Davisil™*

Sample	Temperature (X_1)	Time (X_2)	H_2O (X_3)	Acid (X_4)	Heat (X_5)	Y_1 [a]	Y_2 [b]
PA5	-1	-1	-1	-1	1	1.755	0.736
PA6	1	-1	-1	-1	-1	1.393	0.323
PA7	-1	1	-1	-1	-1	1.392	0.589
PA8	1	1	-1	-1	1	2.029	0.925
PA9	-1	-1	1	-1	-1	2.368	1.233
PA10	1	-1	1	-1	1	1.902	0.76
PA11	-1	1	1	-1	1	2.938	1.43
PA12	1	1	1	-1	-1	2.685	1.2
PA13	-1	-1	-1	1	-1	1.846	0.916
PA14	1	-1	-1	1	1	1.704	0.636
PA15	-1	1	-1	1	1	2.084	0.917
PA16	1	1	-1	1	-1	2.223	0.942
PA17	-1	-1	1	1	1	2.145	0.928
PA18	1	-1	1	1	-1	2.196	0.969
PA19	-1	1	1	1	-1	3.014	1.36
PA20	1	1	1	1	1	3.515	1.49
PA21	0	0	0	0	0	1.666	0.916
PA22	0	0	0	0	0	1.570	0.912
PA23	0	0	0	0	0	1.66	0.905

[a] Y_1 represents response due to weight percentage of Nitrogen atoms per sample.
[b] Y_2 represents response due to the CO_2 uptake in $mmolg^{-1}$ at 1 bar and 298 K

1.3.4.1 Validation of the model

The statistical significance of the model regarding the responses (Y_1, Y_2) was determined by analysis of the residuals as described above. Details of the analysis are found in the paper I. The analysis of the residual showed that the model was very well described regarding the response Y_1, the content of the amine groups. However, the analysis of residuals for Y_2, the CO_2 uptake, showed that the linear model was not sufficient to describe the system. The curvature in this model could be explained with complications from choosing the so-called center points. In Table 2, the center points were the last three experiments and the variables were fixed at levels between low and high. These experiments were replicated to allow the variance and the residuals to be calculated independently from the experimental design. The variance was used for different statistical tests by which the model validation was confirmed. Hence, the choice of the center points is crucial to the model validation. Here, we had two discrete variables, which were fundamentally problematic for the definition of center points. The acid and heat treatment directly affected the number of silanols and silica surface properties, therefore the center points could not exactly be chosen. A precise representation would have included quadratic dependencies; however, for this the number of variables would have had to be decreased (or the number of experiments increased significantly). In Figure 1.13, the experimental responses are plotted versus the calculated to observe whether the curvature had a major effect. The correlation coefficients R^2 were reasonably large. These values indicated that, despite the indications of curvature for the uptake of CO_2 (Y_2), the model could predict the observed data rather well.

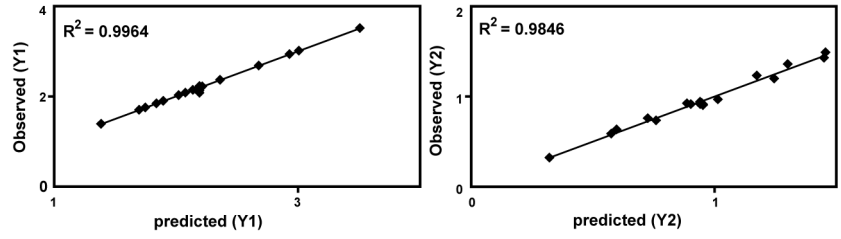

Figure 1.13 *Plots of observed values versus predicted response for APTES modification of Davisil™: a) N-atom content (Y_1); b) uptake of CO_2 (Y_2).*

1.3.4.2 The effect of variables

The calculated effects were determined in the model and are presented in Figure 1.14 with the corresponding estimation of the errors, with respect to both the content of N-atoms and uptake of CO_2. This figure shows that for both responses (Y1, Y2) the amount of water and the reaction time had positive significant effects. Some minor positive effect of the acid treatment was also observed. A range of interaction effects (bilinear terms) usually involving one of the two major effects, influenced the results. These effects are not easy to detect by other approaches. The fractional factorial design allows such higher order effects to be revealed. From the very large variations in the CO_2 uptake among seemingly similar syntheses it is worth the effort to optimize the conditions for post-synthetic modification of Davisil™ with APTES, at least the time of reaction and the amount of water added.

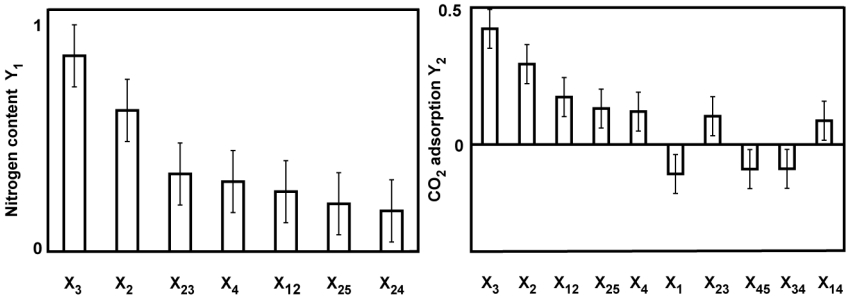

Figure 1.14 *Plot of the most significant effects of the variables (X) on the responses nitrogen content (Y_1) and CO_2 adsorption (Y_2) for APTES modified Davisil™. Interaction effects are double digit.*

The positive effect of water and reaction time on the surface modification with n-propylamine groups can be rationalized by the sol-gel chemistry. The reaction of APTES with the silica surface proceeds with the hydrolysis of the ethoxy groups followed by the condensation among the hydrolyzed APTES and surface silanol groups, see figure 1.15.[61] Both hydrolysis and condensation are time-dependent. The effect of water can be seen from the reactions in Figure 1.15.

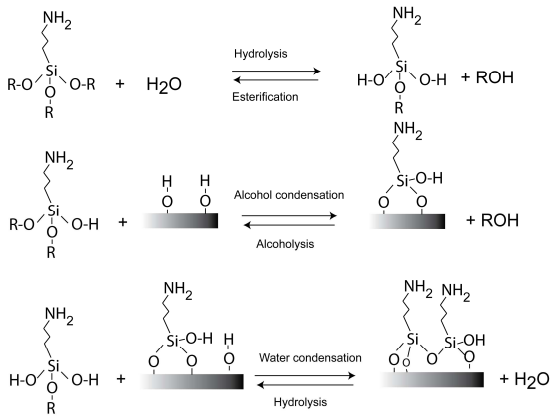

Figure 1.15 *Reaction of the n-propylamine groups with the silica surface. The hydrolyzed alkoxy groups can react either with each other or with the surface silanol groups or both.*

An increased amount of water facilitates hydrolysis of the alkoxygroups, followed by condensation of the groups. This expanded the volume for cross-condensation reactions of APTES and a thicker layer formed on the silica surface.[62,63] The strong dependency on time and amount of water on the uptake of CO_2 and the N-atom content were also consistent with the findings of Harlick and Sayari.[17] They showed that water content is crucial for hydrolysis, condensation, and coating or grafting of the trialkoxy silanes on silica surfaces.

1.3.5 Gas adsorption

Adsorption is the phenomena of adhesion of the atoms, ions or molecules to surface by which the free energy of the system is minimized. Therefore adsorption is always an exothermic process. Gas adsorption involves adhesion of a gas, called adsorptive, into a solid surface, called adsorbent, to form a layer of adsorbed gas or adsorbate. The interaction of the gas with the surface defines the class of the adsorption. We have two types of adsorption on the surfaces:

Physisorption: If the forces between the adsorbent and the adsorbate are physical, e.g. Van Der Waals or electrostatic interactions the adsorption is called to be physisorption.

Chemisorption: In case of formation of chemical bonds, covalent or ionic, between the adsorbate and the adsorbent the adsorption is denoted by chemisorption.

The thermodynamics of adsorption is usually described by a family of curves, isotherms. The amount of adsorbate is correlated to the pressure of an adsorptive gas at a constant temperature. For each isotherm, important information like surface area, pore size, pore volume and pore shapes can be extracted.

1.3.5.1 Surface area and porosity analysis

Surface area is a crucial parameter for optimizing the use of porous material in many applications. However, no single experimental technique can be expected to provide the absolute surface area. Surface area values are therefore of relative nature and should always be related to the method, conditions and the probe molecule used in the measurements. It is generally accepted that nitrogen adsorption at 77K is the standard adsorptive for micro and mesopore analysis.

The standard method for determination of surface area of a substrate is the Braunauer-Emmett-Teller or (BET) method. This method is widely used for the evaluation of the surface areas of the micro- and mesoporous adsorbents. It is based on the following assumptions:

1. All the surface sites have uniform energy of adsorption.
2. No lateral interaction between the adsorbed molecules.
3. Molecules in the first layer act as sites for the molecules in the second layer.
4. Evaporation and condensation properties of all layers above the first layer are similar to the liquid adsorptive.

The original form of BET equation is

$$\frac{V}{V_{mon}} = \frac{C\frac{P}{P^{\circ}}}{(1-\frac{P}{P^{\circ}})(1+(C-1)\frac{P}{P^{\circ}})}, \qquad C = e^{\frac{(\Delta H_A - \Delta H_I)}{RT}}$$

V indicates the volume adsorptive gas at STP, V_{mon} the volume of gas that is required for a monolayer, P° the vapour pressure of the bulk liquid at the same temperature, P the pressure of adsorptive gas and C a constant which is an average energy of adsorption. ΔH_A and ΔH_I are the heat of adsorption and heat of liquefaction respectively. The calculation of surface area is done using the low relative pressures before the condensation of the adsorptive gas. For mesoporous material this region is at relative pressures 0.05-0.35.

1.3.5.2 Effect of surface modification on porosity and Specific surface areas (BET)

The specific surface areas of the studied adsorbents were determined by N_2 adsorption in the BET model. The surface area decreased after coating the Davisil™-silica with APTES, but there was a significant scattering in between the observed surface area and the degree of functionalization, see Figure 1.16. The absence of a trend shows that the degree of homogeneity of the coating varied among the samples synthesized.

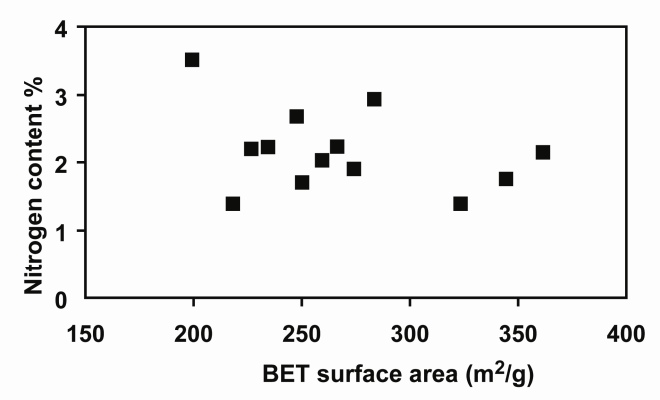

Figure 1.16 *Content of Nitrogen as a function of the BET surface area for APTES modified Davisil™.*

1.3.5.3 Effect of amine surface density on the adsorption of dry CO_2

The adsorption isotherms of CO_2 were determined by volumetric measurements for pure and the propylamine modified silica at room temperature. Adsorption of CO_2 on amine modified silicas occurs by both

physisorption and chemisorption. Physisorption originates from the interaction of the large quadrupole moment of CO_2 with the electrical field variation of the silica surface[64] while chemisorption emerges from chemical reaction of CO_2 with the amine groups to form covalent bonds. As these two interactions are different in strength, resulting in different heat of adsorption, the total uptake of CO_2 on amine modified samples will be affected by the amine surface density. A linear correlation between the total uptake of CO_2, at 25 °C and 760 Torr, and the content of amine groups can be seen in Figure 1.17. This plot shows that the uptake of CO_2 increases when the amine surface density increases. This correlation was expected from a strong influence of chemisorption of CO_2 via ammonium-carbamate ion pairs. It is worth to note that the chemisorption of the CO_2 on amine modified substrates through formation of propylammonium propylcarbamate ion pair follows a linear function below a critical surface density of the amine groups beyond which the uptake increases significantly.

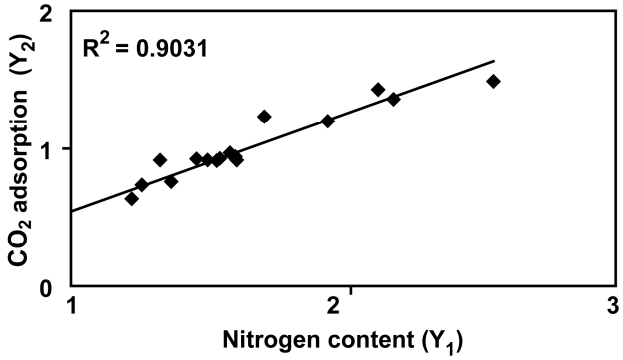

Figure 1.17 *Correlation between the two responses Y_1 (nitrogen content of the samples in mmol/g) and Y_2 (the adsorbed CO_2 in mmol/g), for the APTES modified Davisil™.*

This critical surface density has been reported to be 1 NH_2/nm^2.[42,65,66] However, this behavior is valid at lower pressures in which chemisorption is dominant and the contribution of physisorbed CO_2 is minor. In Figure 1.17 the total uptake of CO_2 comes from both physisorption and chemisorption at high pressure. In which samples with high surface area show significant amount of physisorption. The

contribution of the physisorption can also be seen in that the line does not intercept with origin. The CO_2 uptake on pure mesoporous silica has been shown to be relatively high, due to their high specific surface areas.[48] Knöfel et al. and Bacsik et al. have shown significant amount of physisorption of CO_2 on APTES modified sorbents by macroscopic and spectroscopic techniques.[42,44] Correct calculation of the contribution of the physisorbed CO_2 to the total uptake is impossible by means of volumetric adsorption. IR spectroscopy provides a good method by which the contribution of the physisorbed CO_2 can be calculated at lower pressures. For this reason I have selected four amine modified samples from Table 2 and will discuss their adsorption behavior by both volumetric adsorption and by IR spectroscopy, a detailed description can be found in paper III.

1.3.6 Molecular aspect of amine modified silica and CO_2 adsorption by FTIR spectroscopy

CO_2 is a linear molecule and by definition has 3N-5 or four modes of vibrations in the gaseous state in which N is the number of atoms in the molecule. These modes of vibration are a symmetric and asymmetric stretching along the molecular axis and two bending modes, see Figure 1.18. The symmetric vibration of the CO_2 is IR inactive since the dipole moment of the molecule does not change by this vibration. The asymmetric stretching called (υ_3) absorbs IR radiation at 2340 cm^{-1}. This band has a doublet, there of P and R branching, which is the effect of the vibrational-rotational excitation of CO_2 in the gas phase. The vibrational-rotational band of bending modes, denoted by P, Q and R, of CO_2 shows a triplet band at 667 cm^{-1}. As adsorbed phase the rotation movement of CO_2 disappears and we end up with a single band corresponding to the asymmetric stretching (υ_3) of the CO_2. The IR spectroscopy measurements were conducted in a home made cell to replicate the conditions in the volumetric measurement, for details see experimental section in paper III. The difference is that instead of measuring the uptake of CO_2 at each pressure an IR spectrum was recorded at each pressure. The adsorbed amount of CO_2 on each sample will then be reflected in the band intensities of the formed species.

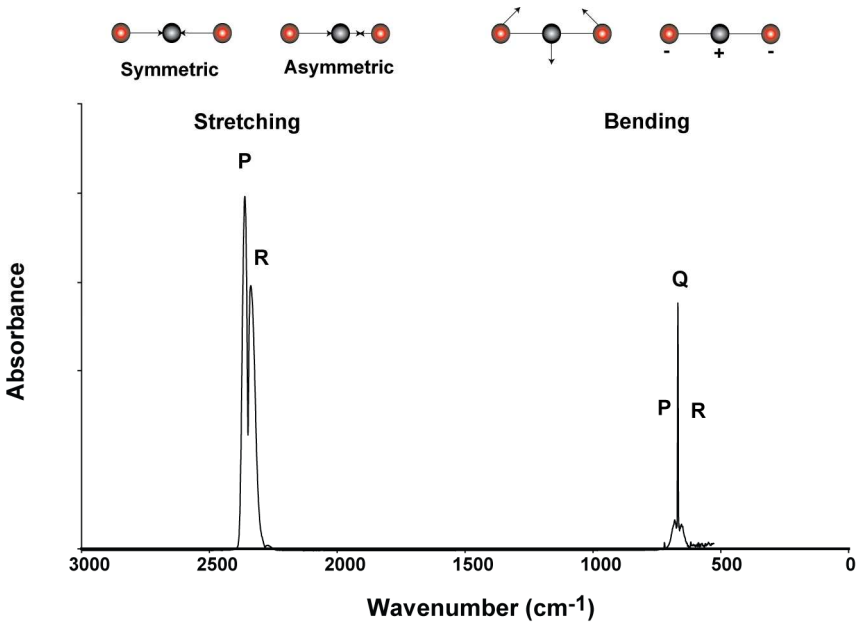

Figure 1.18 *The modes of vibration of CO_2: symmetric and asymetric stretching and the two type of bending. The P, Q and R branching comes form the vibrational-rotational absorption. The asymmetric stretching has no Q branch. The symmetric stretching is IR inactive.(Graph is unpublished and obtained by a spectral resolution of 4 cm^{-1} from gasous CO_2).*

Figure 1.19 shows in situ IR spectra recorded on pure silica and on propylamine modified silicas when contacted with 100 Torr of dry CO_2. Spectra of the sorbents in vacuum condition were used as background spectra to record spectra during CO_2 adsorption measurements. Hence, only changes attributed to CO_2 adsorption are observed in spectra of Figure 1.19. These spectra clearly show that CO_2 adsorbs by physisorption and chemisorption on amine modified samples. The unmodified silica shows only the physisorbed band at 2341 cm^{-1} corresponding to the asymmetric stretching and a negative band corresponding to the change of the vibration of the isolated OH groups on silica surface. This negative band emerged probably because of the hydrogen bonding of these groups with the adsorbed CO_2. The physisorbed CO_2 band can also be seen in amine modified samples with a slight shift since their surface are different in each case. During the

chemisorption CO_2 reacts with the amine groups and the integrity of both molecules are disturbed. This can be seen by the negative band of the NH_2 and CH_2 groups. The most prominent changes are observed though in the multiple bands ranging from 1200-1800 cm^{-1} for propylamine modified silica contacted with CO_2. An exact assignment of the bands in this regime is still a matter of discussion in the literature; however, the latest studies[42,43,47] indicated that the amine groups on the surface of silica form propylammonium propylcarbamate ion pairs and carbamic acid groups. The assignments of these bands can be found in detail in paper III. These spectra show that the band intensities of different species formed by chemisorption increases with increasing the amine content of the samples.

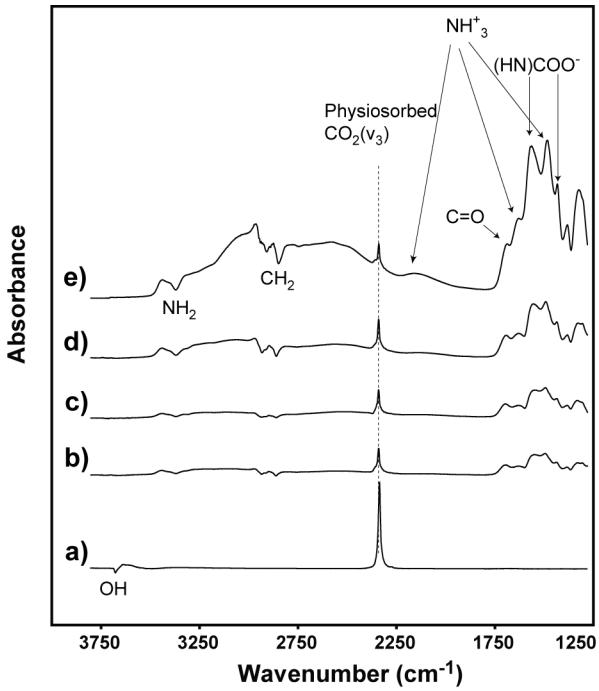

Figure 1.19 *Infrared spectra recorded for a) unmodified silica and propylamine modified davisil™ silica b) PA5(0.87 nm^{-2}), c) PA6(1.37 nm^{-2}), d) PA15(1.64 nm^{-2}) and e) PA20(2.73 nm^{-2}) after equilibration with 100 Torr of pure CO_2. Surface amine density is presented in brackets.*

The relative intensities of the physisorbed bands also differ indicating that the physisorbed amount of CO_2 varies among the samples. The distinct difference of the physisorbed CO_2 band areas can be used to estimate the amount of the physisorbed CO_2 on each sample.

1.3.6.1 Quantification of physisorbed and chemisorbed CO_2

Uptake of CO_2 in amine modified silica occurs by both physisorption and chemisorption as mentioned before. However, a direct quantification of the physisorbed and the chemisorbed amount has not been done before. Figure 1.20 shows the total adsorption isotherms of four amine modified samples with different amine surface density and for unmodified silica.

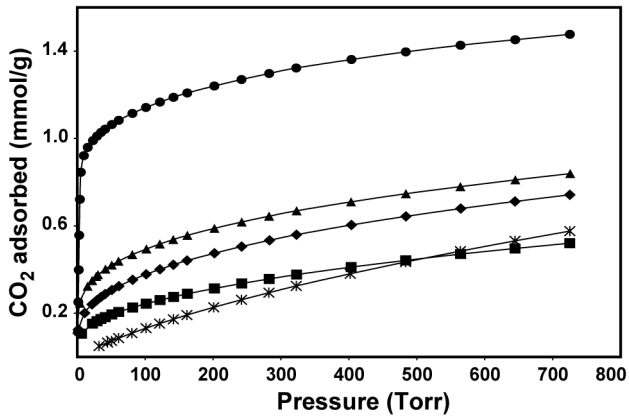

Figure 1.20 *CO_2 adsorption isotherms for pure silica (∗), and propylamine modified davisil™ silicas: PA5 (■)(0.8 mmol/g), PA6 (♦)(1.25 mmol/g), PA15 (▲)(1.5 mmol/g) and PA20 (●)(2.5mmol/g). Measured by volumetric adsorption at a temperature of 23°C. The amine concentration in each sample is presented in brackets.(paper III)*

The amine modified silicas show a higher uptake of CO_2 at low pressures than pure silica indicating that chemisorption is dominant. IR spectroscopy shows that physisorption occurred as well. The IR bands for physisorbed CO_2 are distinctly different from chemisorbed CO_2 species. The area of the ν_3 band of the physisorbed CO_2 (2341 cm^{-1}) is directly proportional to the adsorbed amount of CO_2 and the relation is described by the Beer-Lamberts law ($A = \varepsilon.l.n$) in which the absorption of infrared light A is linearly dependent on the adsorbed amount of CO_2 (n),

the absorption coefficient (ε), and the path length (l). Differences in sample quantities (l) can be compensated by using overtone bands of Si-O-Si vibrations (at 1860 and 2000 cm^{-1}) as internal standards. Pure silica was then used to cross-calibrate the temperature in the FTIR set up and the volumetric adsorption set-up, and to determine the adsorption coefficient (ε). The adsorption coefficients were assumed to be identical for all samples, and the physisorbed amounts were quantified and plotted in paper III, here Figure 1.21.

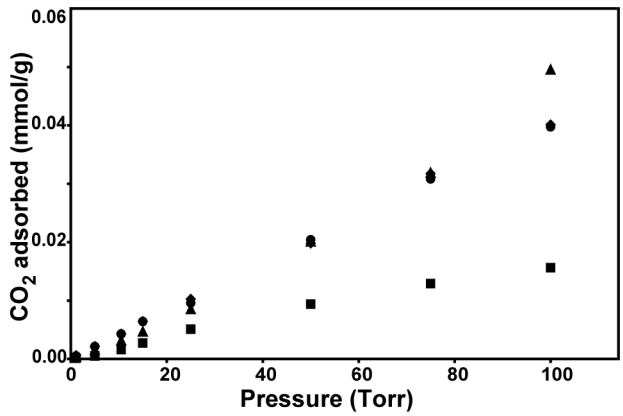

Figure 1.21 *Quantified amounts of physisorbed CO_2 on propylamine modified davisil™ silicas [PA5(♦), PA6(●), PA15(▲) and PA20 (■)].(paperIII)*

This figure displays that PA20, with the highest amount of the amine groups, took up least amount of physisorbed CO_2. What was surprising is the fact that the physisorbed amount of CO_2 did not increase with increasing surface area as it was reported in literature for determining the physisorbed CO_2 on amine modified silicas.[67] However, this observation may show the limitations of using only the surface area for estimating the physisorbed CO_2. The isotherms for chemisorbed CO_2 was calculated by subtracting physisorbed CO_2, as determined from IR spectroscopy, from the total volumetric uptake of CO_2 and plotted in Figure 1.22. The detailed shapes of the adsorption isotherms in Figure 1.22 indicate both that the amount and the distribution of amine groups on the surface of APTES modified samples vary. High CO_2 uptake and high gradient in

the adsorption curve at low pressures (0-10 Torr) correlates with mainly ammonium carbamate ion pair formation, as is evident from the IR spectra. By comparing the slopes of the isotherms for chemisorbed CO_2, it appears as the surface density of the amine groups must be over 2 NH_2/nm^2 to have a significant increase in the amount of ion pairs on CO_2 sorption. This number seems to be specific for this chromatographic silica, or the detailed method for modification of the silica with propylamines.

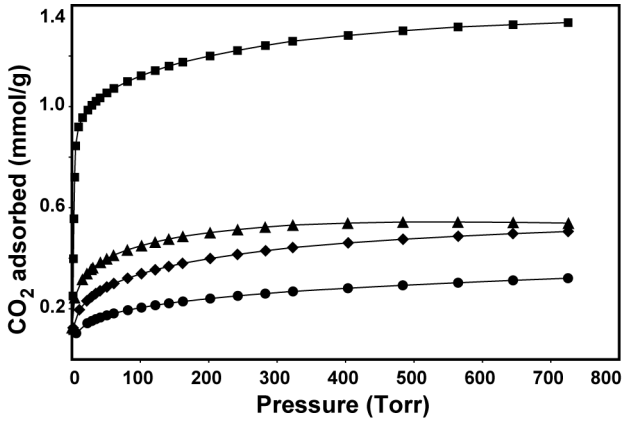

Figure 1.22 *Chemisorbed CO_2 on propylamine modified davisil™ silica PA5(●), PA6(♦), PA15(▲) and PA20 (■). Isotherms were calculated by subtracting the physisorbed amount of CO_2 as established from infrared spectroscopy from the total volumetric uptake of CO_2. (paperIII)*

In case of bicontinuous AMS-6 and MCM-48, SBA-15 around 1 NH_2 group/nm^2 was effective enough to have a high number of ion pairs. We expect that the critical density of amine groups needed for a significant amount of ion pairs to form will vary with curvature, pore size, and with homogeneity in the propylamine modification.

The relative contribution of physisorption and chemisorption is presented in Figure 1.23 for PA5, PA6, PA15 and PA20 at three different pressures. This figure helps in depicting modes of adsorption as a function of propylamine content and pressure. Figure 1.23a and 1.23b shows the adsorption of CO_2 at 10 and 100 Torr respectively. Chemisorption dominates at these pressures for all the propylamine modified sorbents. These pressures are very relevant to potential swing

adsorption processes for a CO_2 removal from flue gas. At the highest pressure physisorption starts to be relevant for the CO_2 uptake on PA5, PA6 and PA15 with comparably small amounts of amine groups, for PA20 with a high amine density physisorption is negligible, most probably because of its rather small specific surface area.

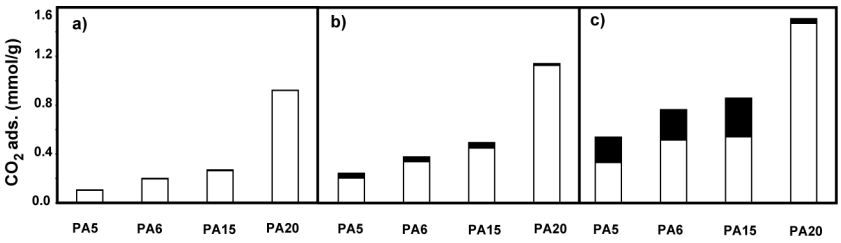

Figure 1.23 *The ratio of the physi- and chemisorbed CO_2 on the propylamine modified davisil™ silica (PA5 (0.87 nm^{-2}), PA6 (1.37 nm^{-2}) PA15 (1.64 nm^{-2}) PA20 (2.73 nm^{-2}) at CO_2 pressures of a) 10.0 Torr (measured), b) 100 Torr (measured) and c) 760 Torr (modelled). The unfilled boxes correspond to the amounts of chemisorbed CO_2, and the filled boxes to the amounts of physisorbed CO_2. Physisorption at 760 Torr has been calculated by Langmuir model. (paperIII).*

1.3.7 Effect of temperature on adsorption capacity and apparent selectivity

The CO_2 adsorption isotherms, in paper III, could very well be described by Freundlich model. In this originally empirical model the amount q adsorbed, relates to the pressure, p, via the heterogeneity parameter n, and proportionality constant, K_f, as:

$$q = K_f p^{1/n}$$

This function has an asymptotic maximum as the pressure increases to high values. The special case of the Freundlich isotherm in which the heterogeneity constant n =1 is referred to as the Henry's law. In this case all the adsorption sites are considered to be equal and there is no lateral interaction between the adsorbed species. The Henry's type of adsorption is usually valid at very low adsorption pressures. Hence the heterogeneity constant n gives an indication about the heterogeneity of the surface. The closer the value is to 1, the more homogenous the surface

is expected to be. The CO_2 adsorption capacity of APTES modified silica decreases with increasing temperature.

Figure 1.24 shows adsorption isotherms of sample PA3 at different temperatures.

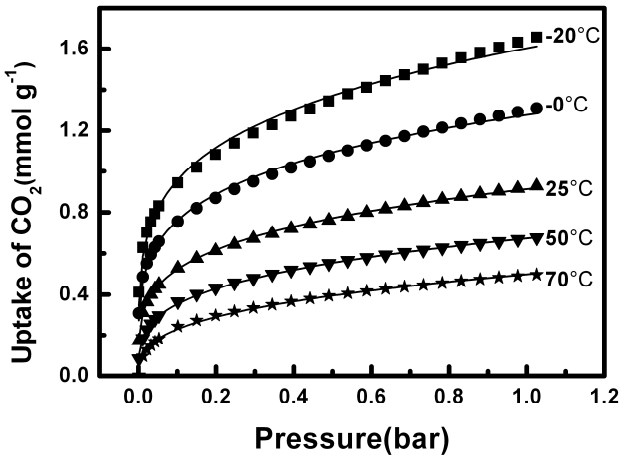

Figure 1.24 *The pressure and temperature dependency of the uptake of CO_2 on DavisilTM silica modified by APTES (PA3). ■ for -20°C; ● for 0°C; ▲ for 25°C; ▼ for 50°C; ★ for 70°C;— the Freundlich expression. (paper II)*

The temperature dependencies of the K_f and n in the Freundlich model has been explained by Urano et al [68]as follows

$$K_f = K_0 \exp(-CRT/\theta_\circ) \text{ and } \qquad \frac{1}{n} = \frac{RT}{\theta_\circ}$$

In this description, $\theta_\circ$ relates to a characteristic adsorption potential. These temperature dependencies indicate that the adsorbed amount of gas will decrease with increasing temperature. We found the logarithm of K_f to decrease linearly with the temperature (T).

The Freundlich model could also be applied to the adsorption of N_2 at the same temperatures. Hence the apparent CO_2/N_2 selectivity could easily be estimated by dividing the Freundlich expressions of the two type of adsorption as follows:

$$S_{ind} = \frac{K_f^{CO_2} p^{1/n_{CO_2}}}{K_f^{N_2} p^{1/n_{N_2}}} = C_a p^{\frac{1}{n_{CO_2}} - \frac{1}{n_{N_2}}} = C_a p^{b_h}$$

For all the samples the apparent selectivity increased with increasing adsorption temperature. Figure 1.25 represents the changes in the apparent selectivity with increasing temperature for APTES modified sample PA3.

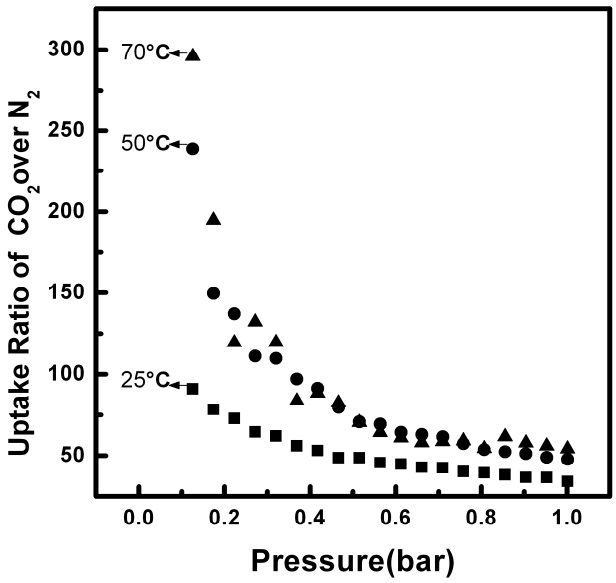

Figure 1.25 *The apparent CO_2/N_2 selectivity as a function of pressure and temperature for a porous silica sample modified with n-propylamine groups (PA3) (■) for 25°C; (●) for 50°C; (▲) for 70°C. (paper II)*

This increase of selectivity could potentially relate to kinetic details in the chemisorption. The stability of the chemisorbed species such as carbamic acid and carbamate ion pairs decrease with temperature. The studied temperature might not be high enough to completely inhibit the formation of these species. Hence, despite low uptake of CO_2 the selectivity is increased simply because the reduction in N_2 uptake is much higher.

1.3.8 Adsorption of wet CO_2 on amine modified silica

Adsorption measurements using humid CO_2 are motivated by the fact that exhaust flue gases usually contain up to 5% water vapour. The humid condition was achieved by purging the dry CO_2 through 2 dm^3 water container and allowing it to saturate overnight. The effect of humid CO_2 on the adsorption capacity of the APTES modified silica was then studied by both volumetric adsorption and by IR spectroscopy. Almost all the APTES modified samples show an enhancement for the uptake of CO_2 when humid conditions were applied. In particular the sample with the highest amount of amine groups (PA20) showed a significant increase in the uptake of CO_2 under humid conditions, see Figure 1.26.

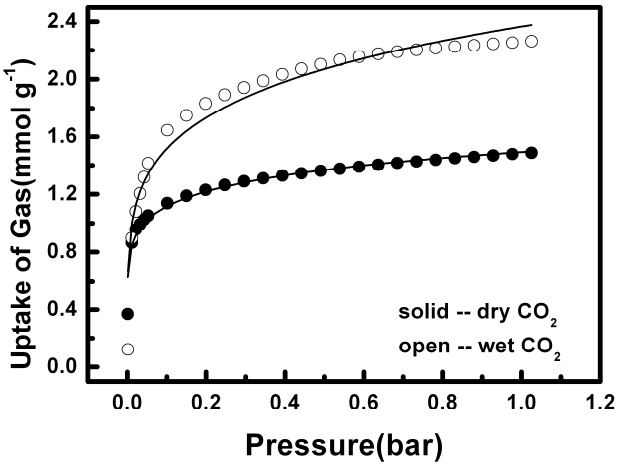

Figure 1.26 *Pressure dependencies of the uptake of the dry (●) and humid (o) CO_2 measured at 25 °C for n-prpoylamine modified sample (PA20).(paper II)*

The rise in the uptake of CO_2 in humid conditions is still a matter of discussion. Without water in the gas, it has been shown that carbamate-ammonium ion pair forms on contacting CO_2 with amine groups on silica. In the presence of water, it has been suggested that the carbamate-ammonium ion pairs reacts further with CO_2 and H_2O, and possibly forms bicarbonate groups.[22] We investigated the uptake of CO_2 under humid conditions by means of IR spectroscopy. APTES modified samples with different amine surface densities were chosen to observe the

differences, see Figure 1.27. The formation of bicarbonate and carbonate species was excluded by the fact that no doubling of the uptake of CO_2 under humid conditions was reached as it was suggested, and no straightforward spectroscopic evidence of bicarbonates could be seen. The changes that could be observed was related to the enhancement of the propylammonium carbamate ion pair bands and the reduction of the C=O stretching of the silylpropylcarbamate.

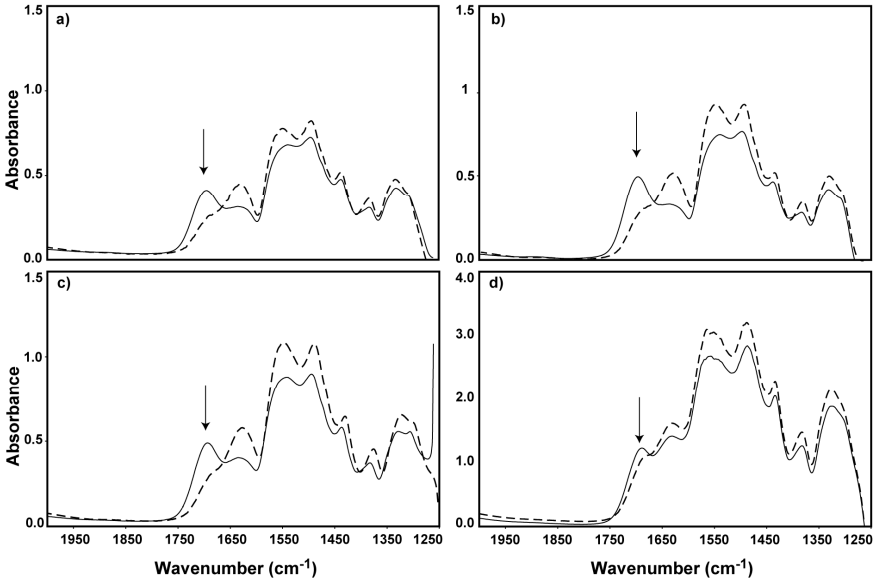

Figure 1.27 *Infrared spectra of the chemisorbed CO_2 region 1200-2000 cm^{-1} when propylamine modified davisil™ silicas are contacted with 760 Torr of dry (solid lines) and humid (dashed lines) CO_2 at room temperature. a) PA5, b) PA6, c) PA15 and d) PA20. (paper III)*

The H-bonded carbamic acid form silylpropylcarbamate with the silanol group by expelling a water molecule. For this reaction to occur very dry conditions are needed, as water hydrolysis ester groups. It can be seen that the relative reduction in the band intensities of the silylpropylcarbamate were higher for the samples with lower amine surface density, indicating that there are a higher fraction of the Carbamic acid that was stabilized by the surface silanol groups. In the samples with higher amine groups, the stability comes from hydrogen bonding to the already formed ammonium carbamate ion pair. The

adsorption of CO_2 and the nature of formed species will then depend on the distribution and surface density of the amine groups. Figure 1.28 represents the difference in the adsorbed species in cases of silicas with high and low amine surface density. However, the enhancement of the CO_2 uptake may be rationalized by the increased number of available amine groups to react with the CO_2. This suggestion comes from the fact that some propyl amine groups are hydrogen bonded to the surface. The presence of water may disturb these hydrogen bonds in a way that they become free to interact with CO_2.

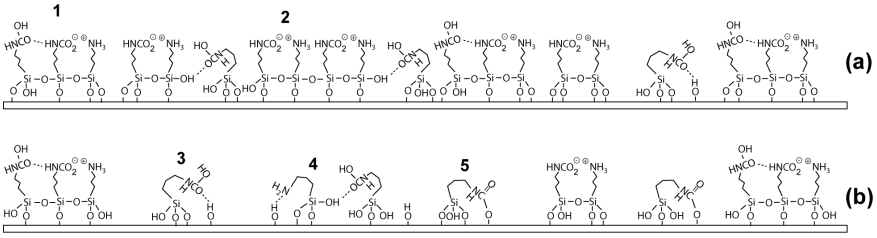

Figure 1.28 *The schematic presentation of the chemisorption of dry CO_2 on propylamine modified silica adsorbents with a) high (2.7 NH_2/nm^2) and b) moderate (0.8-1.6 NH_2/nm^2) amine surface density and formed species. (1) H-bonded carbamic acid to propylammonium propylcarbamate ion pair (2) propylammonium propylcarbamate and (3) H-bonded carbamic acid to surface silanol group (4) H-bonded carbamic acid to surface and residual silanol group and (5) silylpropylcarbamate on amine modified silica samples when subjected to CO_2.*

1.4 Concluding remarks

In this thesis we have investigated amine modified silica, as CO_2 adsorbent. We have shown that this material can be optimized to show rather high uptake and good selectivity. The silica-amine-CO_2 chemistry was studied by IR spectroscopy and for the first time an accurate estimation of the physisorbed amount of CO_2 was done. It is important to note that chemisorption is the dominant adsorption process in these materials at pressures which coincide with pressures of CO_2 in flue gases. The rather large pore dimension of this substrate facilitates mass transport and the low heat capacity of it reduces the regeneration cost. We synthesized silica with different amount of amine groups on the surface exhibiting different adsorption isotherms. With improved adsorption capacity compared to the unmodified silica, these materials can be used in different capturing techniques like pressure swing adsorption PSA or temperature swing adsorption TSA. However, further investigations like the durability and cyclic behaviour of these adsorbents needs to be done.

1.5 References

(1) Brust, O. E.; Sebestia.i; Halasz, I. *J.Chromatogr.* **1973**, *83*, 15–24.
(2) Díaz, J. F.; Balkus Jr, K. J. *J. Mol. Catal. B: Enzym.* **1996**, *2*, 115–126.
(3) Clark, J. H.; Macquarrie, D. J. *Chem. Commun.* **1998**, 853–860.
(4) Fryxell, G. E.; Liu, J.; Hauser, T. A.; Nie, Z. M.; Ferris, K. F. *Chem. Mater.* **1999**, *11*, 2148–2154.
(5) Tokman, N.; Akman, S.; Ozcan, M. *Talanta* **2003**, *59*, 201–205.
(6) Yin, H. P.; Wei, Y. *J. Chem. Soc. Abstr.* **2004**, *228*, U792.
(7) Wen, L. X.; Li, Z. Z.; Zou, H. K.; Liu, A. Q.; Chen, J. F. *Pest Manag.Sci.* **2005**, *61*, 583–590.
(8) Li, Z. Z.; Chen, J. F.; Liu, F.; Liu, A. Q.; Wang, Q.; Sun, H. Y.; Wen, L. X. *Pest Manag.Sci.* **2007**, *63*, 241–246.
(9) Hu, S. H.; Liu, T. Y.; Huang, H. Y.; Liu, D. M.; Chen, S. Y. *Langmuir* **2008**, *24*, 239–244.
(10) Takei, T.; Yonesaki, Y.; Kumada, N.; Kinomura, N. *J. Ceram. Soc. Jpn.* **2009**, *117*, 1180–1185.
(11) Goeppert, A.; Meth, S.; Prakash, G. K. S.; Olah, G. A. *Energy Environ. Sci.* **2010**, *3*, 1949–1960.
(12) Stein, A.; Melde, B. J.; Schroden, R. C. *Adv. Mater.* **2000**, *12*, 1403–1419.
(13) Veltman, K.; Singh, B.; Hertwich, E. G. *Environ. Sci. Technol.* **2010**, *44*, 1496–1502.
(14) Choi, S.; Drese, J. H.; Jones, C. W. *Chemsuschem* **2009**, *2*, 796–854.
(15) Hedin, N.; Chen, L.; Laaksonen, A. *Nanoscale* **2010**, *2*, 1819–1841.
(16) Xu, X.; Song, C.; Andresen, J. M.; Miller, B. G.; Scaroni, A. W. *Energy Fuels* **2002**, *16*, 1463–1469.
(17) Harlick, P. J. E.; Sayari, *Stud. Surf. Sci. Catal.* **2005**, *158*, 987–994.
(18) Zelenak, V.; Halamova, D.; Gaberova, L.; Bloch, E.; Llewellyn, P. *Microporous Mesoporous Mater.* **2008**, *116*, 358–364.
(19) Beck, J.; Vartuli, J.; Roth, W.; Leonowicz, M.; Kresge, C.; Schmitt, K.; Chu, C.; Olson, D.; Sheppard, E.; McCullen, S.; Higgins, J.; Schlenker, J. *J. Am. Chem. Soc.* **1992**, *114*, 10834–10843.
(20) Zhao, D.; Feng, J.; Huo, Q.; Melosh, N.; Fredrickson, G.; Chmelka, B.; Stucky, G. *Science* **1998**, *279*, 548–552.
(21) Hicks, J. C.; Drese, J. H.; Fauth, D. J.; Gray, M. L.; Qi, G.; Jones, C. W. *J. Am. Chem. Soc.* **2008**, *130*, 2902–2903.
(22) Leal, O.; Bolivar, C.; Ovalles, C.; Garcia, J.; Espidel, Y. *Inorg. Chim. Acta* **1995**, *240*, 183–189.
(23) Knowles, G. P.; Graham, J. V.; Delaney, S. W.; Chaffee, A. L. *Fuel Process. Technol.* **2005**, *86*, 1435–1448.
(24) Kim, S.; Ida, J.; Guliants, V.; Lin, J. *J. Phys. Chem. B* **2005**, *109*, 6287–6293.

(25) Khatri, R. A.; Chuang, S. S. C.; Soong, Y.; Gray, M. *Energy Fuels* **2006**, *20*, 1514–1520.
(26) Serna-Guerrero, R.; Da'na, E.; Sayari, A. *Ind. Eng. Chem. Res.* **2008**, *47*, 9406–9412.
(27) Chaffee, A. L.; Knowles, G. P.; Liang, Z.; Zhany, J.; Xiao, P.; Webley, P. A. *Int. J. Greenhouse Gas Control* **2007**, *1*, 11–18.
(28) Angeletti, E.; Canepa, C.; Martinetti, G.; Venturello, P. *J. Chem. Soc.- Trans.* **1989**, 105–107.
(29) Harlick, P. J. E.; Sayari, A. *Ind. Eng. Chem. Res.* **2007**, *46*, 446–458.
(30) Harlick, P.; Sayari, A. *Ind. Eng. Chem. Res.* **2006**, *45*, 3248–3255.
(31) Franchi, R. S.; Harlick, P. J. E.; Sayari, A. *Ind. Eng. Chem. Res.* **2005**, *44*, 8007–8013.
(32) Franchi, R.; Harlick, P.; Sayari, A.; Jaroniec, M., *Stud. Surf. Sci. Catal.* 2005; Vol. 156, pp. 879–886.
(33) Chen, C.; Yang, S.-T.; Ahn, W.-S.; Ryoo, R. *Chem. Commun.* **2009**, 3627–3629.
(34) Zhao, G. Y.; Aziz, B.; Hedin, N. *Appl. Energy* **2010**, *87*, 2907–2913.
(35) Aresta, M., Ed.; 2010. *Carbon Dioxide as Chemical Feedstock*.
(36) Alauzun, J.; Besson, E.; Mehdi, A.; Reye, C.; Corriu, R. J. P. *Chem. Mater.* **2008**, *20*, 503–513.
(37) Bossa, J.-B.; Borget, F.; Duvernay, F.; Theulé, P.; Chiavassa, T. *J. Phys. Chem. A* **2008**, *112*, 5113–5120.
(38) McCann, N.; Phan, D.; Wang, X.; Conway, W.; Burns, R.; Attalla, M.; Puxty, G.; Maeder, M. *J. Phys. Chem. A* **2009**, *113*, 5022–5029.
(39) Zhang, Y.; Chen, H.; Chen, C.-C.; Plaza, J. M.; Dugas, R.; Rochelle, G. T. *Ind. Eng. Chem. Res.* **2009**, *48*, 9233–9246.
(40) Glasscock, D. A.; Critchfield, J. E.; Rochelle, G. T. *Chem. Eng. Sci.* **1991**, *46*, 2829–2845.
(41) Masuda, K.; Ito, Y.; Horiguchi, M.; Fujita, H. *Tetrahedron* **2005**, *61*, 213–229.
(42) Knöfel, C.; Martin, C.; Hornebecq, V.; Llewellyn, P. L. *J. Phys. Chem. C* **2009**, *113*, 21726–21734.
(43) Danon, A.; Stair, P. C.; Weitz, E. *J. Phys. Chem. C* **2011**, *115*, 11540–11549.
(44) Bacsik, Z.; Atluri, R.; Garcia-Bennett, A. E.; Hedin, N. *Langmuir* **2010**, *26*, 10013–10024.
(45) Pinto, M. L.; Mafra, L.; Guil, J. M.; Pires, J.; Rocha, *J. Chem. Mater.* **2011**, *23*, 1387–1395.
(46) Aziz, B.; Zhao, G.; Hedin, N. *Langmuir* **2011**, *27*, 3822–3834.
(47) Bacsik, Z.; Ahlsten, N.; Ziadi, A.; Zhao, G.; Garcia-Bennett, A. E.; Martin-Matute, B.; Hedin, N. *Langmuir* **2011**, *27*, 11118–11128.
(48) Belmabkhout, Y.; Sayari, A. *Adsorpt.-J. Int. Adsorpt. Soc.* **2009**, *15*, 318–328.
(49) Xu, X.; Song, C.; Miller, B. G.; Scaroni, A. W. *Ind. Eng. Chem. Res.* **2005**, *44*, 8113–8119.
(50) Xu, X.; Song, C.; Miller, B. G.; Scaroni, A. W. *Fuel Process. Technol.* **2005**, *86*, 1457–1472.
(51) Athens, G. L.; Shayib, R. M.; Chmelka, B. F. *Curr. Opin. Colloid Interface Sci.* **2009**, *14*, 281–292.
(52) Babonneau, F.; Yeung, L.; Steunou, N.; Gervais, C.; Ramila, A.; Vallet-Regi, M. *J. Sol-Gel Sci. Technol.* **2004**, *31*, 219–223.

(53) Epping, J. D.; Chmelka, B. F. *Curr. Opin. Colloid Interface Sci.* **2006**, *11*, 81–117.
(54) Garcia-Bennett, A. E.; Brohede, U.; Hodgkins, R. P.; Hedin, N.; Stromme, M. *Langmuir* **2007**, *23*, 9875–9881.
(55) Ek, S.; Iiskola, E.; Niinisto, L.; Pakkanen, T.; Root, A. *Chem. Commun.* **2003**, 2032–2033.
(56) Ek, S.; Iiskola, E.; Niinisto, L.; Vaittinen, J.; Pakkanen, T.; Root, A. *J. Phys. Chem. B* **2004**, *108*, 11454–11463.
(57) Zhuravlev, L. T. *Colloids. surf., A* **2000**, *173*, 1–38.
(58) Box, G. E. P.; Hunter, W. G.; Hunter, J. S. *Statistics for experimenters: an introduction to design, data analysis, and model building*; Wiley, 1978.
(59) Carlson, R.; Carlson, J. E. *Design and optimization in organic synthesis*; Elsevier, 2005.
(60) Lundstedt, T.; Seifert, E.; Abramo, L.; Thelin, B.; Nystrom, A.; Pettersen, J.; Bergman, R. *Chemom. Intell. Lab. Syst.* **1998**, *42*, 3–40.
(61) Blumel, J. *J.Am.Chem.Soc.* **1995**, *117*, 2112–2113.
(62) Osterholtz, F.; Pohl, E. *J. Adhes. Sci. Technol.* **1992**, *6*, 127–149.
(63) Brinker, C. J.; Scherer, G. W. *Sol-gel science: the physics and chemistry of sol-gel processing*; Gulf Professional Publishing, 1990.
(64) Roque-Malherbe, R.; Polanco-Estrella, R.; Marquez-Linares, F. *J. Phys. Chem. C* **2010**, *114*, 17773–17787.
(65) Young, P. D.; Notestein, J. M. *ChemSusChem* **2011**, *4*, 1671–1678.
(66) Hiyoshi, N.; Yogo, K.; Yashima, T. *Microporous Mesoporous Mater.* **2005**, *84*, 357–365.
(67) Serna-Guerrero, R.; Belmabkhout, Y.; Sayari, A. *Chem. Eng. J.* **2010**, *161*, 173–181.
(68) Urano, K.; Koichi, Y.; Nakazawa, Y. *J. Colloid Interface Sci.* **1981**, *81*, 477–485.

Chapter 2

Calcium Carbonates

2.1 Introduction

It is not a bold statement that calcium carbonate is one of the most important minerals that directly influences life on our planet. It comprises an important part of the carbon cycle.[1] Many applications have been found due to its low cost and benign properties.[2–7] Carbon dioxide dissolves in water and forms carbonic acid and further bicarbonate and carbonate ions. The latter reacts with calcium ions and produces calcium carbonate. It is fascinating that such simple chemical reactions influence life in such a great manner. Virtually all calcium carbonate deposits in the oceans are formed by organisms. Organisms such as corals, molluscs, and algae in shallow waters, and foraminifera and coccoliths (algae) in the open ocean use calcium carbonate in their shells to enhance their defence mechanisms.[8–11] The variation of the unique and beautiful morphologies distinguish biogenic calcium carbonate rather than simple inorganic crystal morphologies. These morphologies indicate that the organisms, in elegant ways, are able to control the nucleation and growth of calcium carbonate. Inspired by how nature controls crystallization of calcium carbonate, researchers try to mimic such a process in designing new materials. In doing so, different types of additives, both organic and inorganic, have been used in crystallization of calcium carbonate, which has resulted in interesting morphologies.[12,13] However, a better understanding of the role additives play requires insight into the crystallization of calcium carbonate from ionic solutions. Recent research has been preoccupied with understanding the nucleation, growth and transformation of calcium carbonate from an amorphous phase.[14–18] New concepts such as mesocrystals, prenucleation clusters and polymer induced liquid precursors have been introduced, which seriously challenged the belief that calcium carbonates are formed according to the classical view of crystallization.[19–22] According to the classical view of crystallization, nuclei of sufficient sizes forms from supersaturated solutions and grow bigger as ions attach one by one. In the modified view of crystallization, calcium carbonate crystals form largely by aggregation of nano-particles of calcium carbonate. Clusters of calcium

carbonate aggregate to nano scaled amorphous phase, which in turn aggregate and transform into larger crystalline entities. The roles of macromolecules in this view are defined by their interaction with either clusters or colloidal particles as well as with ions in solution.

2.1.1 Calcium carbonate precipitation

The equilibrium system of the carbonate buffer can be written as:

$$CO_2 + H_2O \Leftrightarrow H_2CO_3 \Leftrightarrow HCO_3^- + H^+ \Leftrightarrow CO_3^{-2} + 2H^+$$

The concentration of carbonic acid is very low at room temperature and atmospheric pressure; therefore it can be neglected in studies where precipitation of calcium carbonate is performed by mixing two ion sources. The acid constants are given by pKa1 = 6.35 and pKa2 = 10.33. The concentrations of bicarbonate and carbonate ions are therefore highly pH dependent. The consequence of this pH dependency is reflected in the pH regimes in which the concentrations of carbonate ion allow formation of calcium carbonate, see figure 2.1.

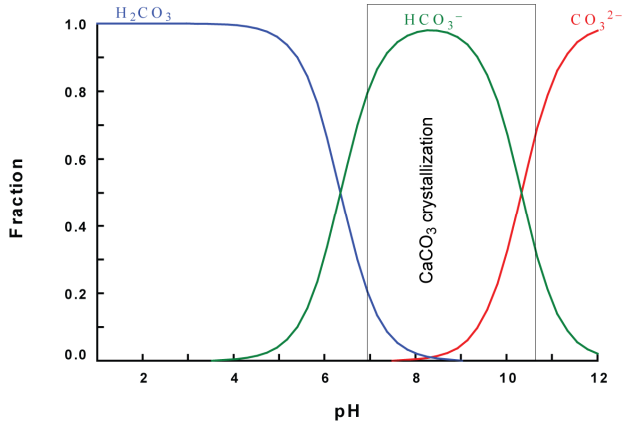

Figure 2.1 *Mole fractions of different carbonate species as a function of pH. Diagram created from software Medusa for chemical equilibrium systems by Ignasi Puigdomenech from Royal Institute of Technology.*

Crystallization of calcium carbonate reduces the concentration of carbonate ions and by that the pH. Therefore, it is important to record or keep the pH constant. The pH can be controlled by adding hydroxide ions or by using buffered solutions. Constant pH keeps the super

saturation level approximately constant, and precipitated or crystallized phases can be rationalized easier than if the pH varied.

Calcium carbonate, in addition to its transient amorphous phase, has three anhydrous polymorphs; vaterite (spheroids), aragonite (rod like) and calcite (rhombohedra). Calcite is the thermodynamically stable phase in most conditions. These polymorphs have different crystal structures and chemical and physical properties. Crystallization of calcium carbonate is usually proceeded by the Ostwald's step rule.[23,24] This rule states that crystallization follows a kinetic path. The least dense polymorphs forms first, and is followed by subsequent transformations into thermodynamically stable phases. Figure 2.2 illustrates the reaction pathway of transformations of calcium carbonates according to Ostwald's step rule.

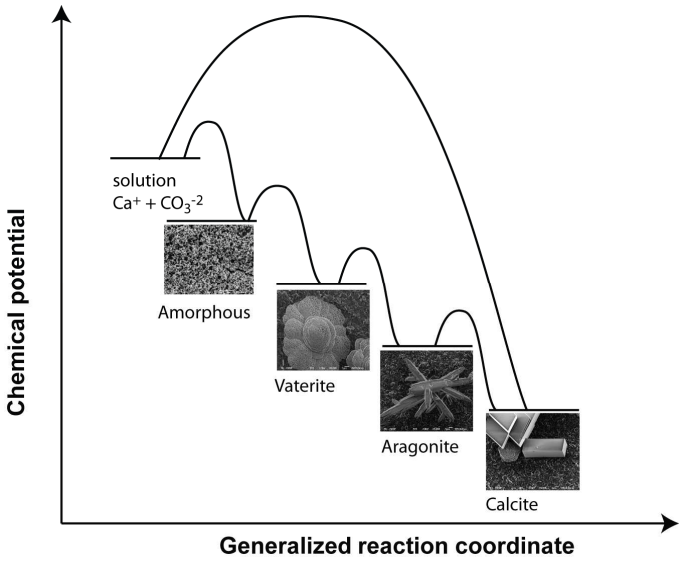

Figure 2.2 *Kinetic pathway of crystallization of calcium carbonate according to the Ostwald's step rule and corresponding morphology of the polymorphs.*

The crystallization pathways of calcium carbonates do not necessarily proceed as they are described in figure 2.2. For example, aragonite is difficult to nucleate and, usually, precise experimental conditions are needed to synthesize this polymorph.

2.1.2 Amorphous calcium carbonate (ACC)

ACC is a highly transient phase that without stabilization transforms into the crystalline forms. It lacks the long range order and does not diffract X-rays or electrons. Organisms use highly soluble ACC as a temporary reservoir for crystallization, and in some cases to enhance the mechanical properties because of its isotropic nature.[14,25–27] ACC can be stabilized by proteins[28], different polymers[20,29–33], or magnesium ion.[34] Structural analysis of such stabilized ACC exhibit similarities to the three anhydrous crystalline form of $CaCO_3$.[35,36] The question is then if the structural features of different types of ACC are influenced by the additives or are in fact intrinsic properties of ACC. For this reason, we precipitated ACC without the addition of any additives. Such transient ACC have previously been synthesized by rapid mixing from concentrated solution or by synthesis at low temperatures.[37,38] In this thesis we stabilized these phases by changing the solvent polarity, which produces a high super saturation. The low solubility of the solvent hinders the ripening process and stabilizes the amorphous character of the precipitate.

2.1.3 Role of additives

A variety of organic and inorganic additives have been used to understand how organisms control crystallization of calcium carbonate .[12,39,40] Molecules with anionic functional groups have been used to modify polymorphism and morphology in the majority of studies. In most descriptions, the role of additives has been limited to complexation with ions or adsorption to crystalline faces inhibiting/promoting the growth of crystals in a certain direction. In this way, the different morphologies of obtained crystals were explained. However, discovery of the pre nucleation clusters and polymer induced liquid precursors (PILP) casted doubt on such a simplified mechanism.[20,21] The role which additives play is still not fully understood, but recent studies suggest new mechanisms. Gebauer et al. suggested that additives can interact on different levels.[41] They suggested nine different types of interactions that might occur involving organic additives. Here I list these interactions. On ionic level, additives can adsorb the ions in a solution thus creating an

inhomogenous distribution of the ions or reducing the free ion concentration and inhibition of nucleation. They can also interact with the formed clusters and alter the equilibrium conditions. On larger nanoparticular scales, they can stabilize nano-particles by adsorption or stabilize the local structure of the amorphous or crystalline nano-particles. Adsorbed additives on nano-particles can also modify the interaction between particles thus influencing oriented attachment or vectorial alignment in formation of, for example mesocrystals. The nano-particles wrapped by additives become stable against Ostwald ripening through shielding from solution.

In my view the type of interaction that additives insert will depend on the synthetic condition such as temperature, pH, polymeric and ionic concentration. In this thesis we investigated the combined effects of additives and experimental conditions and obtained particles with interesting morphologies.

2.2 Experiments and methods

2.2.1 Materials

For syntheses the following substances were used: calcium chloride hexa hydrate (Sigma-Aldrich 99% [7774-34-7]), sodium bicarbonate (Sigma-Aldrich 99.7% [144-55-8]), tris (hydroxymethyl) aminomethane (TRIS; Aldrich [77-86-1]), a high molecular anionicpolymer, poly (acrylamido-2-methylpropanesulfonic acid) (PAMPS; Alrdich [27119-07-9], M_w 2000000), and Millipore™ water.

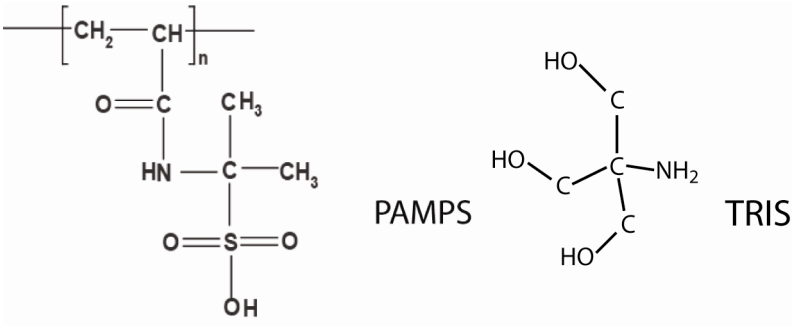

2.2.2 Synthesis of amorphous calcium carbonate (ACC)

Synthesis of amorphous calcium carbonate was performed at two pH values; 8.75 and 9.8. A commercial titration device Metrohm Titrino 712DMS and in house made titration software was used to keep the pH constant and read out the data for synthesis at 20 ± 3°C. Solutions of calcium chloride (10mM) were added at controlled rates using a syringe pump to carbonate buffer 10 mM prepared at each pH. Solutions were poured slowly into 2L of ethanol (99.95%) before nucleation and precipitation. The precipitated transient phase was collected by centrifugation after aging for 2h, a more detailed description of the experimental condition can be found in paper V.

2.2.3 Synthesis of crystalline calcium carbonate

Synthesis of crystalline calcium carbonate was conducted at constant pH values 8.1 using TRIS (0.2M) as buffering agent. Buffered solutions of calcium chloride and sodium bicarbonate were mixed at controlled addition rate. Stirring rate was controlled by a LabasscoTM mechanical stirrer and temperature was kept constant by a VWR heat controller model 1136-1D. Detailed conditions of the experiments can be found in paper IV. A schematic illustration of the experiment setup can be seen in Figure 2.3.

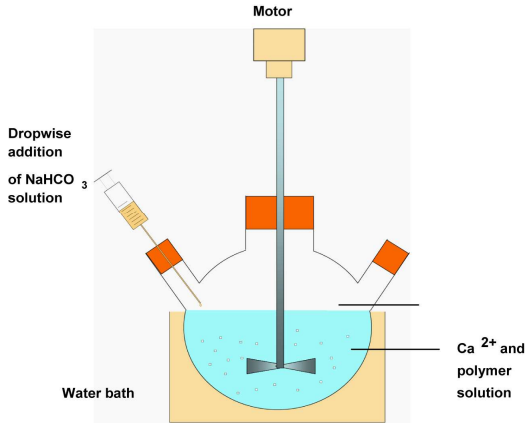

Figure 2.3 *The experimental set up for crystallization of calcium carbonate under controlled pH, temperature and stirring conditions.*

For clarification I list the experiments:

a) Time dependent synthesis of calcium carbonate without additive at two stirring rates (1000 rpm and 150 rpm). (T = 70 °C, pH=8.1)

b) Time dependent synthesis of calcium carbonate with PAMPS as the additive at two stirring rates (1000 rpm and 150 rpm). (T = 70 °C, pH=8.1)

c) Temperature dependent synthesis, 25, 40 , 60 and 90 °C with PAMPS as additive. (Stirring rate 1000 rpm, pH 8.1).

d) pH dependent studies at 7.0, 7.5 and 8.1 with PAMPS as additive (Stirring rate 1000 rpm, T = 25 °C)

e) PAMPS concentration synthesis at 0.25 w%, 0.5 w% and 1.0 w% from the total solution. (pH = 8.1, T = 25 °C and stirring rate 1000 rpm).

Beside PAPMS a number of other additives such as poly acrylic acid with different molecular mass were also used. I present only some of the interesting observations in this thesis.

2.2.2 Powder X-ray diffraction (PXRD)

For the XRD experiments, we employed an X'Pert PANanalytical diffractometer with an X'Celerator detector. Patterns were recorded in the range 5-70° (2θ) and were analyzed with the X'Pert HighScore Plus program.

2.2.5 Electron microscopy

Scanning electron microscopy SEM was measured on a JEOL JSM7000F microscope in SEI mode. Samples were not sputtered. The acceleration voltage applied was varied from 0.8 to 3 KV. Transmission electron microscopy TEM was performed at room temperature on a JEOL JEM-2100 microscope equipped with a LaB_6 gun operated at 200 kV. ACC dispersions in acetone were dropped on Cu TEM grids with holey carbon films and dried in air. In order to minimize beam damage, a weak electron beam with a current density lower than 0.1 pA/cm^2 was used. It is worth noting that the electron beam was impossible to observe on the florescent screen by naked eye. TEM observation and image acquisition were performed utilizing a Gatan SC1000 ORIUS CCD camera. SAED patterns were acquired utilizing a Gatan ES500W Erlangshen CCD camera.

2.2.6 IR spectroscopy

FTIR spectra of fine-ground, neat powder samples were recorded on a Varian 670-IR spectrometer, equipped with an attenuated total reflection (ATR) detection device (Goldengate by Specac with diamond ATR element and KRS-5 lenses) and a room temperature detector of deuterated triglycine sulfate (DTGS).

2.3 Results and discussion

In this section we will follow the Ostwald's step rule of crystallization. First we will discuss the formation of amorphous $CaCO_3$ and show that they have different structures, which is from paper V. The second study is on the formation of crystalline $CaCO_3$ and its dependence on experimental conditions will be explained, which is from paper IV.

2.3.1 The "structure" of amorphous $CaCO_3$ (ACC)

Two distinct types of ACC were precipitated by controlling the pH of the solution. The choice of the pH values was based on earlier studies by Gebauer et al. They have reported that the binding energy of the Ca^{2+}-CO_3^{-2} ion pair decreases when increasing pH, which allows formation of the less stable polymorph, in this case, vaterite.[42] Quenching of the precipitate before transformation into the crystalline phase will allow us to see whether the ACC phases have different short range order.

2.3.1.1 ^{13}C NMR of the ACC

Aspects of local environment of the carbonate ions in amorphous phases of $CaCO_3$ can be revealed by ^{13}C NMR spectroscopy. Spectra of two ACC's show clearly different features (see Figure 2.4.). In this figure the two amorphous phases, pc-ACC and pv-ACC give rise to two distinct broad peaks. The corresponding crystalline sharp peaks of calcite and vaterite are shown as the dashed peaks.

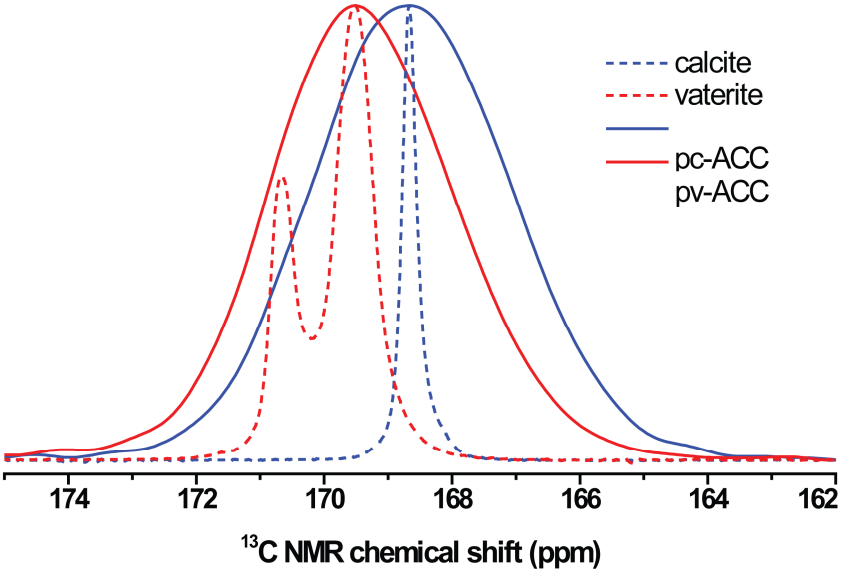

Figure 2.4 *^{13}C solid-state NMR spectra recorded by single pulses at a magnetic field of 9.4 T and a MAS rate of 8.0 kHz. The identical position of the NMR peak maximum observed from each amorphous phase and its crystalline counterpart highlights their close structural similarity over an atomic length-scale up to a few Å around the carbon atom.(paper V)*

Vaterite showed two crystallographically distinct carbonate ions with a ratio of 1:2 resonating at a ^{13}C NMR chemical shift 170.7 ppm and 169.5 ppm, whereas calcite showed a single crystallographic site resonating at 168.5 ppm. The Gaussian shape of the ^{13}C NMR peaks reflected the structural disorder of the two amorphous phases. The average chemical shift of the pc-ACC coincides well with that of crystalline calcite, suggesting a closely related structure. The average chemical shift of the pv-ACC coincided with the primary peak of vaterite at 169.5 ppm, suggesting that the second minor peak evolved during the crystallization of the pv-ACC to crystalline vaterite.

2.3.1.2 IR spectroscopy of ACC

The characteristic bands of ACC have been reported in literature as 1455-1480/1396-1427 cm^{-1} (doublet v_3), 1065-1075 cm^{-1} (v_1) and 862-873

(v_2).[34,37,43–46] The v_1 bands relates to symmetric stretching, the v_2 band to the out of plane bending, the v_3 band to the anti-symmetric stretching and the broad v_4 band to the planar bending of the carbonate group. A schematic illustration of the carbonate vibration modes is shown in Figure 2.5.

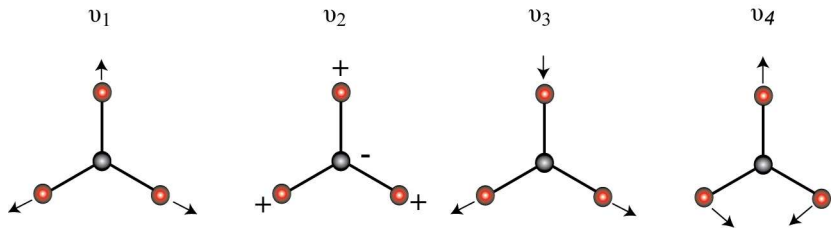

Figure 2.5 *vibration modes of carbonate groups in calcium carbonate,* υ_1 *is symmetric stretching,* υ_2 *out of plane bending,* υ_3 *anti-symmetric stretching and* υ_4 *is planar bending of the carbonate group.*

The IR spectra of the two amorphous phases are presented in Figure 2.6. The frequencies at the different band maxima and the shapes of different bands of the two amorphous phases accord well with the reports in literature. IR spectroscopy shows sensitivity toward differences in short range order in amorphous solids. Hence the difference in possible short-range structure can be observed in the band details. The IR spectra for the two amorphous phases show a shift in the frequencies of the bands v_1, v_2 and v_4 in addition to appearance of a broad band at 1026 cm^{-1} in the spectrum of pv-ACC. The corresponding crystalline phases are shown as dashed spectra. The v_1 band for pv-ACC is slightly shifted (1070 cm^{-1}) compared to the same mode of stretching for pc-ACC (1074 cm^{-1}). In a prefect crystalline calcite this band is missing, since there is no dipole moment change during this vibration. In pc-ACC this band is visible, which is due to disturbance of the bond angles or orientations of the carbonate group. This figure is helpful in illuminating the difference between the two amorphous phases.

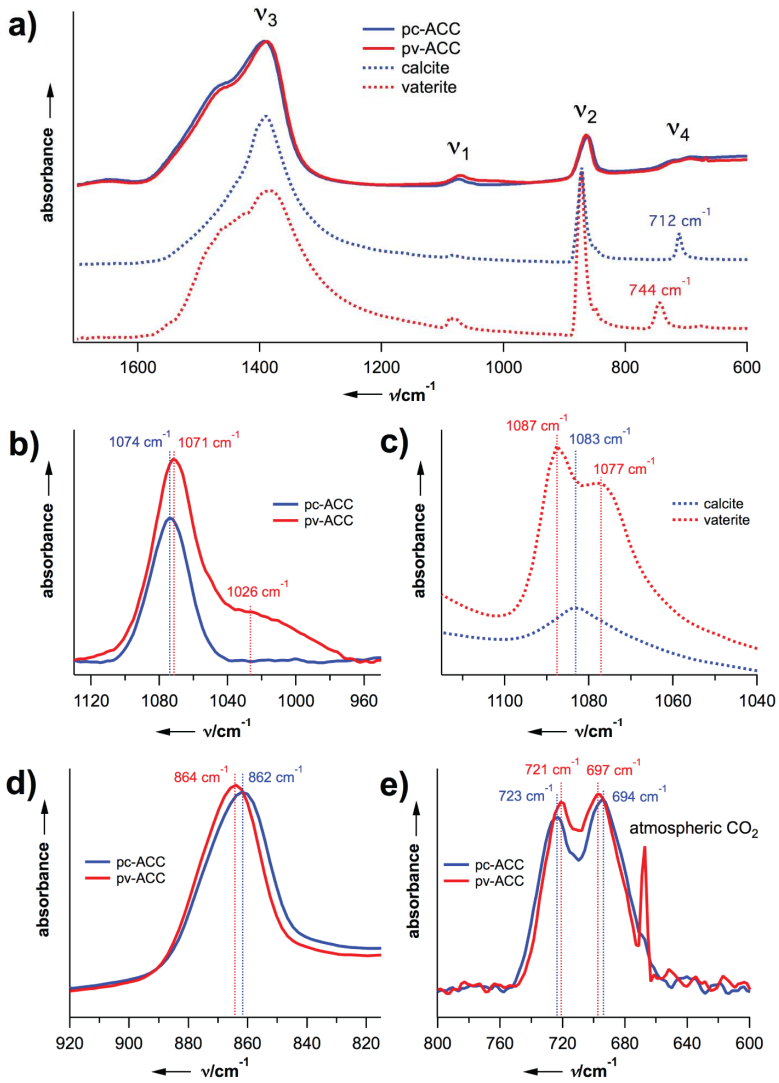

Figure 2.6 *IR spectra of proto calcite ACC pc-ACC and proto vaterite pv-ACC as indicated. a) Overview of the* $\upsilon_1, \upsilon_2, \upsilon_3$ *and* υ_4 *bands. b)* υ_1 *band for pc-ACC and pv-ACC. c)* υ_1 *band for calcite and vaterite. d)* υ_4 *band for pc-ACC and pv-ACC. e)* υ_4 *band for calcite and vaterite. The minor sharp band at 667* cm^{-1} *corresponds to atmospheric* CO_2*. IR clearly shows that the ACC phases are devoid of any organic additive (paper V).*

2.3.1.3 Morphology and particle size determination of ACCs

The particle sizes of the two amorphous phases were determined by electron microscopy and by small angle x-ray scattering SAXS, this data is presented in paper V. Figure 2.7 shows micrographs from SEM and TEM of the two amorphous phases. SEM micrographs of the pc-ACC and pv-ACC (Figure 2.7 A, B) show that they are structured differently on the colloidal length scale. Spherical aggregates of ~20nm can be seen for pv-ACC while pc-ACC shows larger aggregated spheroids in the size range 30-100 nm. Note that the electron beam in SEM tended to crystallize the hydrated and highly transient pv-ACC. TEM micrographs reveal the size of the underlying particles, see Figure 2.7 C-F. The underlying particles in pc-ACC tended to form larger aggregates (marked with white arrows in Figure 2.7C) than the pv-ACC. High resolved TEM images show that the aggregates consist of small and partially fused particles of 1-2 nm in size, see Figure 2.7 E-F. The size of the underlying particles is in good agreement with the size of the thermodynamically stable pre-nucleation clusters.[21] The amorphous nature of the two samples could be seen by the electron diffraction as well as by X-ray diffractograms (not presented here).

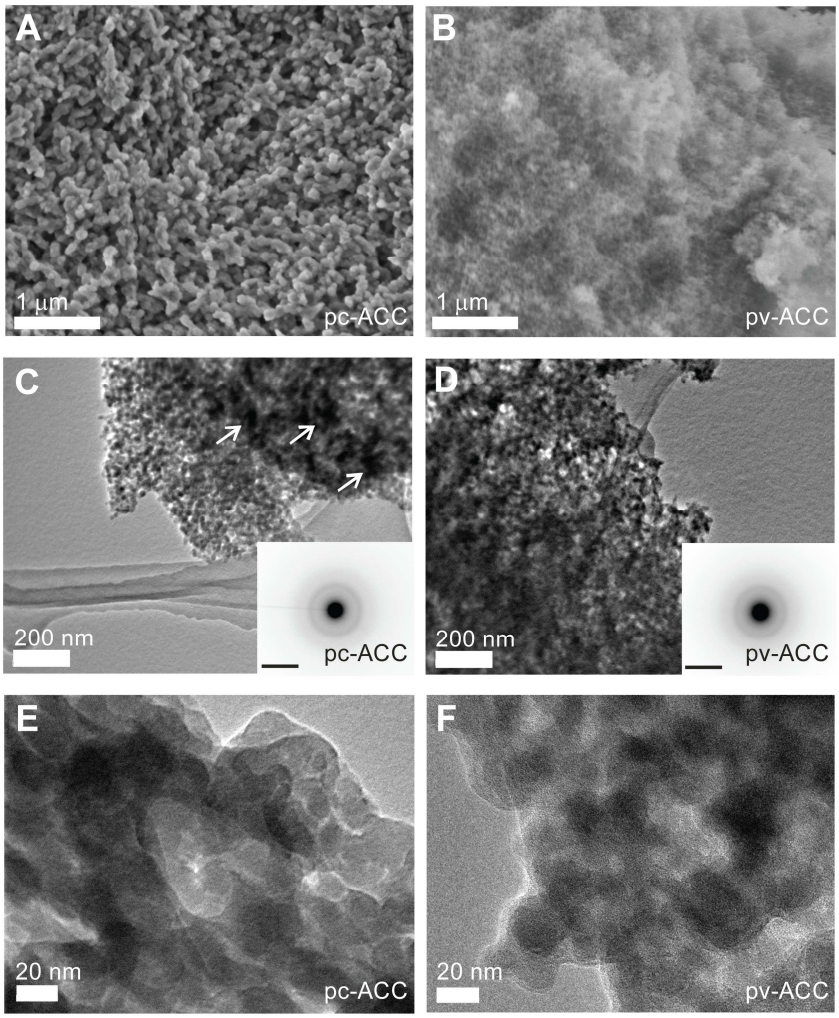

Figure 2.7. *Electron microscopy analyses of pc-ACC and pv-ACC as shown. A, B: Scanning electron microscopy SEM images; C-F Transmission electron microscopy TEM images. Insets in C and D are diffractograms, which represent electron diffraction (ED) obtained from an area slightly larger than the particular image sections, and show the amorphous character of the samples, ED scale bars: 5 nm^{-1}. The diffraction images are shown as negatives in order to make weak features clear.(paper V)*

2.3.2 Crystalline $CaCO_3$

2.3.2.1 Stirring rate dependency of the additive-free $CaCO_3$ crystallization

The time evolution of $CaCO_3$ polymorphs were followed in reactions conducted under mixing using stirring rates of 150 rpm and 1000 rpm. $CaCO_3$ was synthesized by controlled addition of a $NaHCO_3$ solution to a $CaCl_2$ solution (both solutions were buffered at pH 8.1). Samples were removed from the reactions and worked up for further characterization. Crystalline forms of $CaCO_3$ were identified by powder X-ray diffraction (XRD), and relative amounts determined by Rietveld refinements.

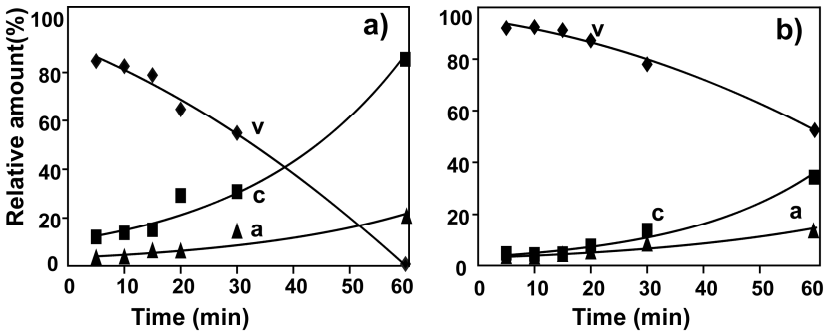

Figure 2.8 The time evolution of relative amounts of precipitated $CaCO_3$ polymorphs: vaterite(♦),calcite(■) and aragonite(▲) a) stirring rate of 150 rpm and b) stirring rate of 1000 rpm. The reaction temperature was 70 °C.(paper IV)

These amounts are plotted vis-à-vis time in Figure 2.8a for stirring at a rate of 150 rpm and in Figure 2.8b for stirring at a rate of 1000 rpm. For both stirring rates applied, vaterite was the dominate polymorph during the early stages. Initially, more calcite and aragonite formed under mixing with a rate of 150 rpm as compared with a rate of 1000 rpm. Transformations of vaterite to aragonite and calcite occurred more rapidly under slow stirring compared to rapid. Under stirring at 150 rpm all vaterite had transformed within 60 minutes. Under mixing at 1000 rpm, the majority of phase was still vaterite after 60 minutes.

There are two main points; first, the difference between the amount of vaterite at early stages of the reaction, and second, the rate of

transformation of vaterite into other polymorphs. In our opinion aggregation mediated crystallization[19] could rationalize these findings. The crystallization pathway of $CaCO_3$ has been shown to proceed via aggregation of pre-nucleation clusters into amorphous phase from which the crystalline phase can form.[19,47] It has been shown that all three polymorph can form in parallel from the amorphous phase.[16] The initial distribution of ACC phases should be similar as the reaction conditions, besides the stirring rate, were equal. At the early stages of the reaction large amounts of vaterite formed, which is consistent with the Ostwald's step rule. However, these amounts were much higher when using a higher stirring rate. Hypothetically, at high stirring rates, attachment of primary particles to calcite and aragonite may be more inhibited than vaterite or the growth of vaterite may be assisted by the convective currents as opposed to the growth of calcite and aragonite. These metastable phases dissolved for the ultimate benefit of the stable calcitic phase, all according to the Ostwald step rule. The solubility's of these metastable phases were higher than that of calcite. Hence, the concentrations of calcium and carbonate ions were higher than the ionic concentration required for calcitic growth. These metastable phases were in excess, which indicted that it was unlikely that the dissolution of the metastable particles inhibited the growth of calcite. High stirring rate facilitated the mass transport and could have sped up the transformation. However, the transformation was slower at higher stirring rates than at lower rates, indicating that neither the dissolution of the metastable phases nor the flux supplying the growth of the calcite were rate-limiting processes. An inhibition of the aggregation of the primary particles into calcite by stirring rate might explain the slower transformation rates into calcite. Simply, nano-scaled pre-calcitic particles dissolved before aggregating into large and stable particles.

2.3.2.2 Stirring rate dependency of $CaCO_3$ crystallization with additive

Synthesis with PAMPS as additive was performed at high and low stirring rates. Some calcite formed to a somewhat higher amount at low stirring rates compared to high stirring rates. The amount of vaterite was high under conditions of high and low stirring rates, see paper IV.

Thermal gravimetric analysis (not shown here) showed that $CaCO_3$-PAMPS precipitate contained up to 6 wt% polymer, indicating that the polymer had a role in stabilizing the metastable phase. The formation of amorphous $CaCO_3$ was confirmed at the early stages of the reaction. We detected ACC with PAMPS in the reaction. By quenching the sample just seconds after the reaction in liquid nitrogen followed by subsequent freeze-drying we prevented the transformation into crystalline phases. Figure 2.9 shows SEM micrograph of the amorphous phase in which typical spherical particles[37] in the size range of 20-200 nm could be observed.

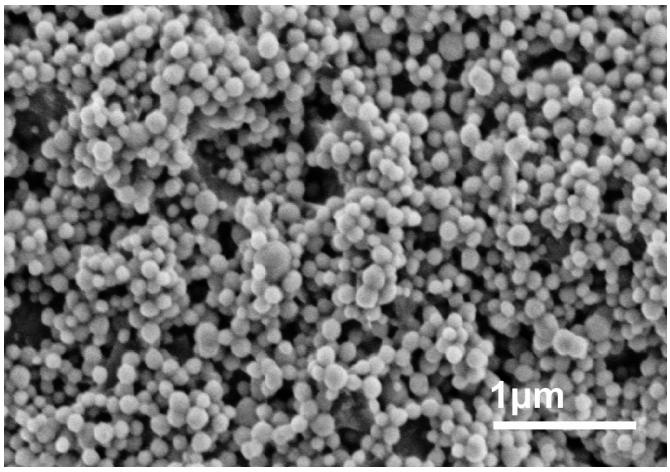

Figure 2.9 *Scanning electron microscopy SEM image of amorphous $CaCO_3$, quenched in liquid N_2 just seconds after the start of initiating the reaction followed by freeze-drying (paper IV).*

The impact of the stirring rate was observed in the size of the aggregates. Vaterite aggregates were about 10 times larger at higher stirring rates than aggregates at lower stirring rates initially, see Figure 2.10 a and b. The difference in size could be related to the higher collision frequency of particles at high stirring rates, resulting in large aggregates. The semi-spherical morphology was common for aggregates in both cases. The sizes of the sub-particles in the aggregates in both cases were in the same range as the amorphous particles presented in Figure 2.9, for details see paper IV. The hypothesis that large particles would have grown as an effect of enhanced ion diffusion by high stirring rates can be rejected.

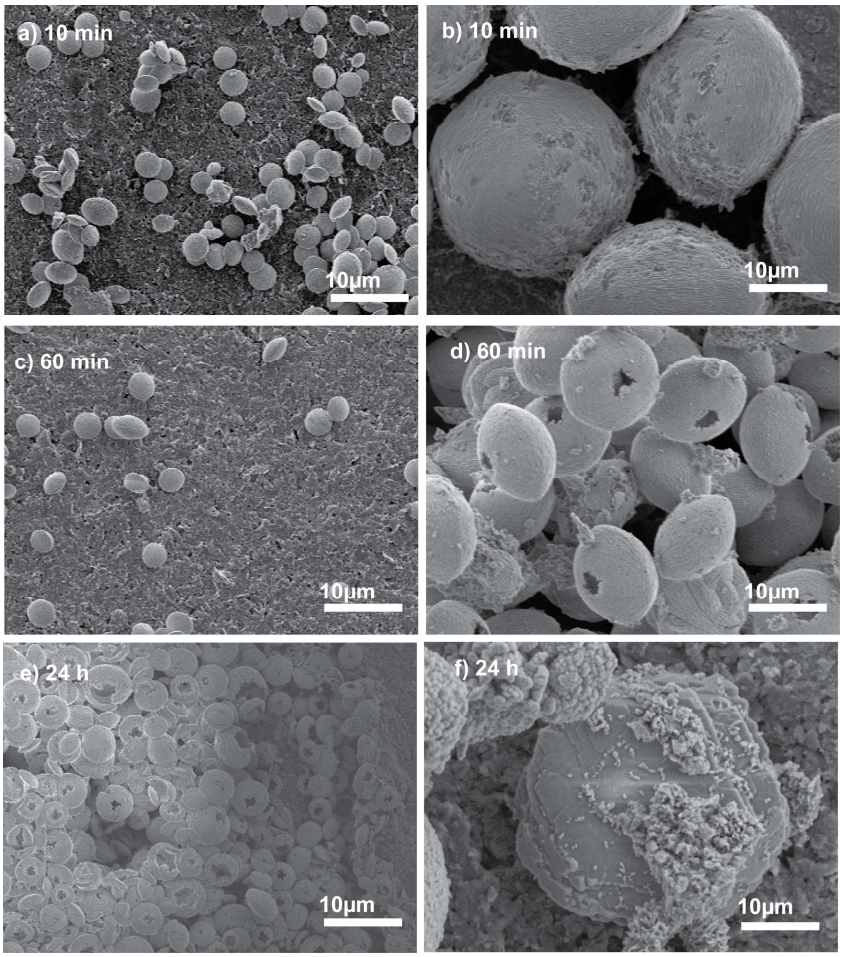

Figure 2.10 Scanning electron microscopy SEM images of vaterite synthesized at 70 °C with PAMPS as additive. Left column (stirring at 150 rpm): a) after 10 min; c) after 60 min; and e) after 24 hours additional aging at stagnant condition. Right column (stirring at 1000 rpm): b) after 10 min; d) after 60 min; and f) after 24 hours additional aging at stagnant condition. Note the size differences of aggregates in the left and right columns (paper IV).

No transformation of the vaterite to other phases was observed under stirring conditions, but when samples were brought to stagnant conditions and allowed to age, the aggregates started to transform into

calcite by dissolution and precipitation. The rate of transformation at stagnant condition was higher for aggregates obtained under conditions of higher stirring rates than under conditions of lower stirring rates. The higher stirring rate might have caused fast and energetically unfavourable aggregation of sub-particles compared to such aggregation under lower stirring rates. Aggregating nano-particles had more time to reorient themselves into energetically favourable directions under conditions of slow stirring rates. Hence, disintegration of the small sub-particles was easier compared to the aggregates formed at low stirring rates.

2.3.2.3 Effect of temperature

$CaCO_3$ was synthesized with PAMPS as additive at four different temperatures. The obtained aggregates were analyzed by SEM and XRD. The reaction temperatures were 25°C, 40°C, 60°C, and 90°C. Phase analysis by XRD showed that the amount of vaterite increased by increasing the reaction temperature. The sizes of the underlying sub-particles were calculated by the Scherrer equation and showed that these sizes increase by increasing the reaction temperature, see Figure 2.11.

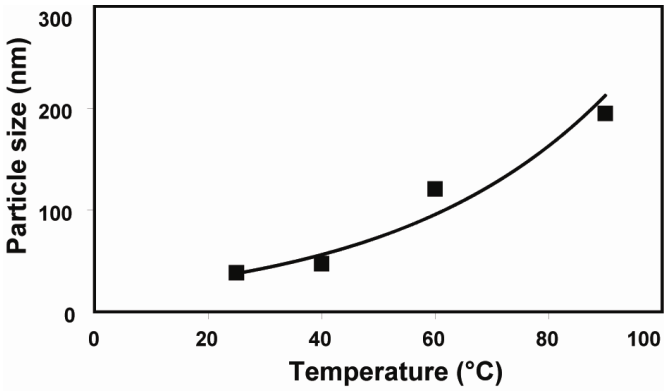

Figure 2.11 *Average grain/nano particle size of the particles constituting the aggregates of vaterite versus the reaction temperature. Sizes were calculated from X-ray powder diffraction XRD data using the Scherrer equation.*

In a self consistent picture the nano-particles/grains of vaterite exhibit growth driven by microscopic dependencies that include effect from diffusion, surface energies and curvatures. These processes accelerate at high temperatures due to increased diffusivities as well as relative increased stability of vaterite.[48] I believe that the impact of the temperature on the size of the nano-particles is reflected in the morphology of the aggregates. The morphologies of the aggregates depend on the combinational effect of additive and reaction conditions, see Figure 2.12. The aggregates had hollow spherical morphologies at 25°C, Saturn-like spheres at 40°C, hexagonal layered at 60°C and irregular shaped at 90°C. What is interesting is that some of these morphologies have been reported in literature to be a result of specific interaction of a special polymer.[49,50]

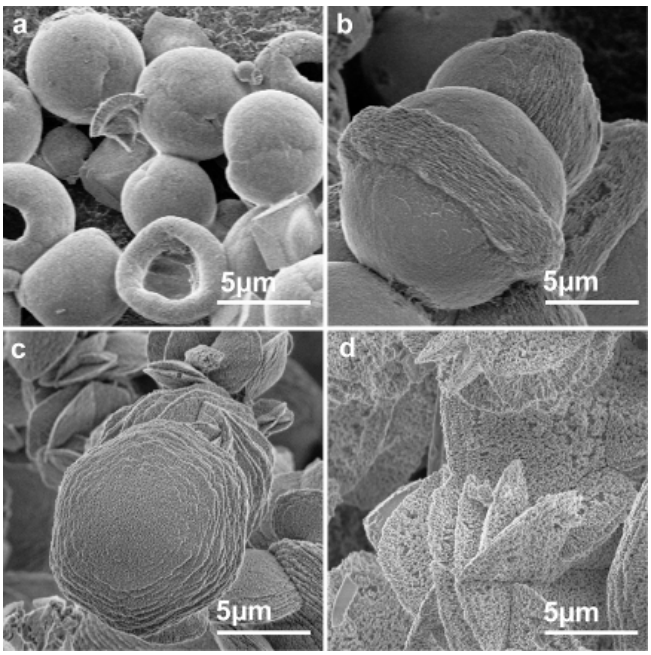

Figure 2.12 *SEM images of aggregates of $CaCO_3$ synthesized under rapid stirring 1000 rpm in the presence of poly(acrylamido-2-methylpropanesulfonic acid) PAMPS at different temperatures a) 25 °C, b) 40 °C, c) 60 °C and d) 90 °C. The samples were collected after one hour of reaction (paper IV).*

The change in morphology was not only limited to vaterite particles, but was also reflected to the calcite obtained after aging the sample, see Figure 2.13. This figure shows the morphologies of calcite at 25°C and at 60°C. Also these morphologies have been observed by others in completely different systems.[51] In our view, the interaction of the polymer is important but not determinant in selection of the underlying nano-particle size and morphology. For example, the hexagonal or hexagonal-like unit cell of vaterite was expressed macroscopically on the aggregates at 60°C. This morphology was then preserved under transformation to calcite on a local level.

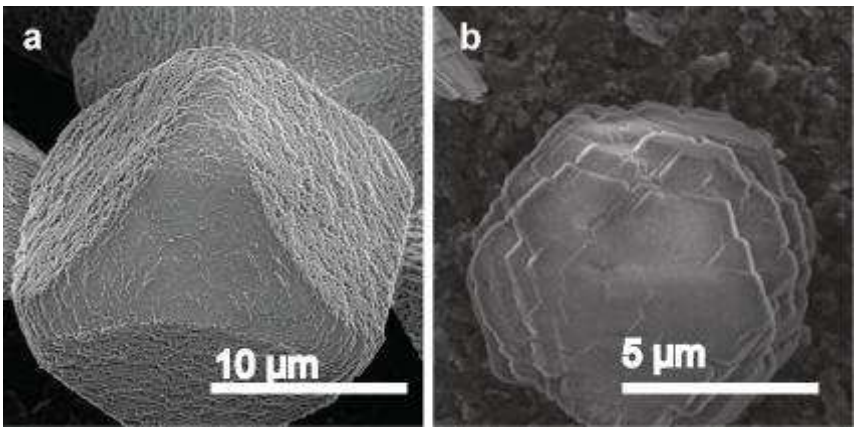

Figure 2.13 *Scanning electron microscopy SEM images of aggregated calcite particles synthesized and aged for 24 hours at a) 25 °C and b) 60 °C. The solutions were subjected to rapid stirring (1000 rpm) for one hour and poly(acrylamido-2-methylpropanesulfonic acid) PAMPS was used as additive (paper IV).*

2.3.2.4 Effect of pH

We studied particles formed at pH 7.0 and 7.5 in addition to the pH 8.1 presented in 2.3.2.3. The reactions were conducted at 25°C and a mixture of calcite and vaterite phase was obtained. Different morphologies were observed for these two pH conditions. Oblatic aggregates of vaterite together with truncated cubes of calcite could be found at pH 7.0, see Figure 2.14. While the aggregates of vaterite at pH 7.5 showed similar

Saturn-like morphology as was observed at higher temperatures. This observation yet again indicated that very specific interaction was not necessary to synthesize particles with complicated morphology, but could be modulated by changes in, for example, pH.

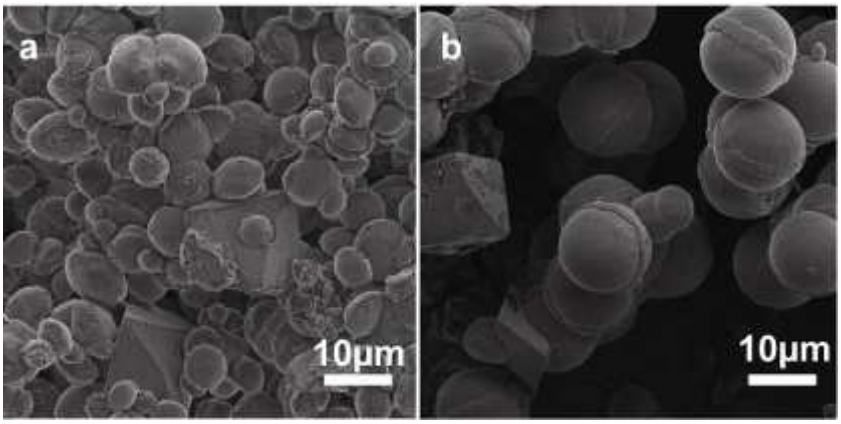

Figure 2.14 *Scanning electron microscopy SEM images of aggregates of $CaCO_3$ synthesized using high stirring 1000 rpm and with poly(acrylamido-2-methylpropanesulfonic acid) PAMPS as additive. The particles were synthesized at a) pH 7.0 and b) pH 7.5, at 25 °C and one hour of rapid mixing (1000 rpm) (paper IV).*

2.3.2.5 Effect of polymer concentration

The importance of polymer concentration was studied at three concentrations; 0.25 w% and 0.5 w% in addition to 1 w% (in total solution) presented in section 2.3.2.4. As expected, mixtures of calcite and vaterite formed at all PAMPS concentrations. The amounts of vaterite increased with increasing polymer concentration, indicating the vaterite stabilizing effect of PAMPS. Vaterite aggregates had spherical morphologies with some Saturn-like spheres at higher polymer concentration, see paper IV.

2.4 Proposed mechanism for crystallization of $CaCO_3$

We propose a self consistent mechanism that rationalizes the findings in paper IV-V for the crystallization of $CaCO_3$ from solutions, see Figure 2.15.

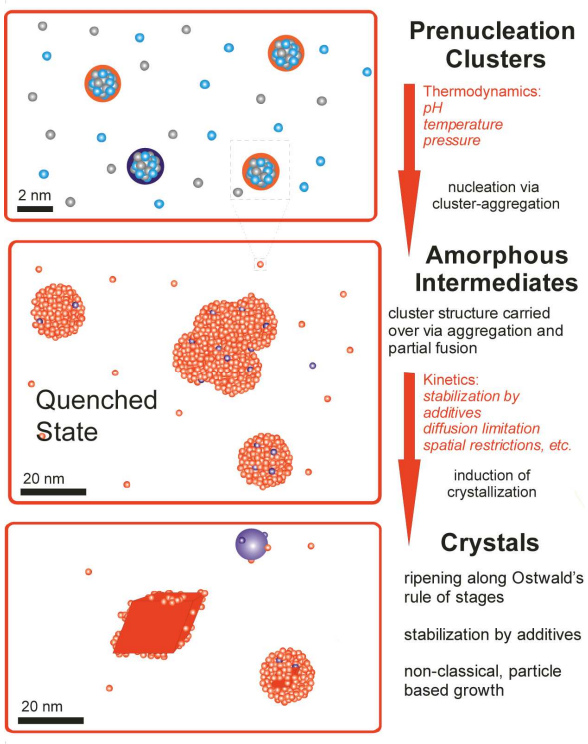

Figure 2.15 *Proposed mechanism of $CaCO_3$ crystallization at low super saturation Before nucleation, clusters with vateritic (blue) and calcitic (red) short-range ordering form. The partitioning of the different clusters depends on the conditions of the solution (here pH). pc-ACC forms via aggregation and partial fusing of the precursor clusters into 20 nm-sized spheres. By quenching in ethanol a phase interface is established and the concentration of ions and clusters decreases The particles of ACC aggregate and fuse together. (The illustration is taken from paper V).*

$CaCO_3$ starts to form with formation of clusters with distinct structures before nucleation.[21] These clusters aggregate and partially fuse into either

pc-ACC or pv-ACC during nucleation. Experimental conditions such as temperature and pH might play a significant role in the selection of clusters or small particles. In particular, pH showed to be decisive in selection of the two types of clusters, which resulted in either pv-ACC or pc-ACC. Aggregation of different types of clusters or nano-particles of amorphous phase seemed to be affected by stirring rate. Nano-particles of pv-ACC seemed to aggregate faster than pc-ACC under high stirring conditions. Additive, in paper IV PAMPS, had a stabilization effect of the vaterite nano-particles regardless of the stirring rate. This stabilization was kinetic in nature and aggregates transformed to calcite under stagnant conditions.

2.5 Sidetracks

2.5.1 Effect of asymmetry in the Ca^{2+}/ CO_3^{2-} ratio.

In studying the asymmetry in the Ca^{2+}/ CO_3^{2-} ratio, the TRIS buffer was not used. We used condition of pH 8.1 and PAMPS concentration 1 w%. Ca^{2+}/ CO_3^{2-} ratios of 1:2, 1:1 and 2:2 were used, whereas the total ion concentration was kept constant at 0.1 M. The effect of ratio can be observed in the morphology of the vaterite aggregates, see Figure 2.16.

Figure 2.16 *The morphological changes of vaterite as a result of the change in the Ca/CO3 ratio. From left to right Ca^{2+}/ CO_3^{2-} ratio 1:2, 1:1 and 2:1 (not published).*

The change in morphologies were, in this case, related to the size of the underlying sub-particles, see Figure 2.17.

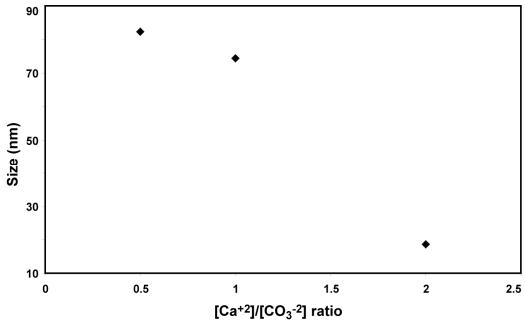

Figure 2.17 *The change in the sub-particle size calculated from X-ray data by Scherrer equation as a function of the Ca^{2+}/ CO_3^{2-} ratio used in the synthesis of calcium carbonate by using PAMPS as additive (not published).*

These sizes speculatively relates to the complexing power of PAMPS. At small Ca^{2+} concentrations PAMPS complexes Ca^{2+} ions. Hence, the effective superstauration is low at low Ca^{+2} concentrations and the formed particles tend to be large. Small particles were formed when the Ca^{2+} concentrations were significantly higher. The size of underlying particles seemed to affect the final morphology of the aggregate. The same behaviour was seen when different morphologies were obtained by changing the synthesis temperature.

2.5.2 Effect of chain length in Polyacrylic acid-Calcium carbonate system

In these syntheses, polyacrylic acid (PAA) with different chain lengths were used as additives. The syntheses were performed at the same conditions as for PAMPS, (Buffered at pH 8.1, high stirring 1000 rpm, but at room temperature). The calcium chloride solution was mixed with PAA, which formed a white Ca-polymer complex followed by the addition of $NaHCO_3$. The PAA with long and intermediate chain lengths formed a gel-like transparent precipitate which turned to a glass like object upon drying. Similar composite material has been reported by Kato et al.[52] Temperature dependent X-ray analysis showed that this glass transformed to calcite at the temperatures of the PAA combustion, see Figure 2.18. The first assumption was that the pc-ACC was stabilized by PAA and when PAA was burned off it transformed to calcite. However, attempts to study the ^{13}C enriched samples with ^{13}C NMR showed no presence of carbonate species. We believe that the glassy composite is Ca^{2+}- PAA complex which at elevated temperatures might form $CaCO_3$.

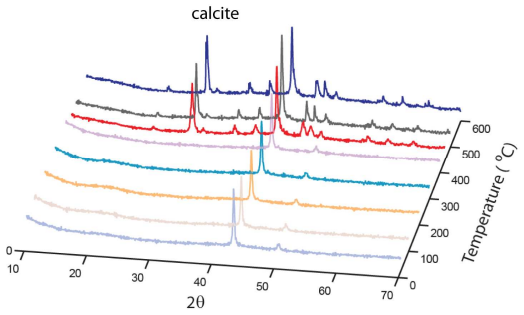

Figure 2.18 *Temperature dependent X-ray diffractograms of glassy composite "$CaCO_3$-PAA". Samples were placed on a steel holder while heating under dry air. The peaks at 43° and 50° come from the steel holder. The otherwise X-ray transparent composite shows X-ray diffractogram of calcite at 500°C at which polyacrylic acid (PAA) is completely burned off (not published).*

PAA with short chain length showed completely different effects. Conical formed aggregates of calcite were obtained. The morphology of these aggregates was similar to $BaSO_4$ reported in literature[53], see Figure 2.19.

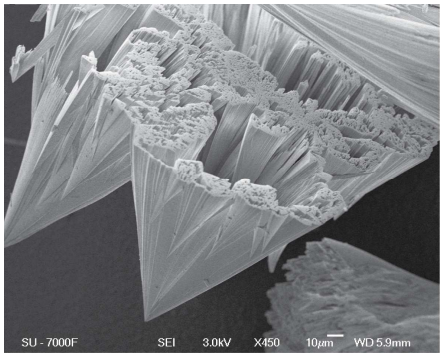

Figure 2.19 *Scanning electron microscopy SEM images of Conical calcite aggregates obtained from synthesis of $CaCO_3$ with PAA with short chain length (Mw = 1800) (not published).*

The space group of $BaSO_4$ crystals are Pcmn, which is the same as the aragonite. These distinct morphologies suggest some form of oriented attachment of the nano-particles of calcite. At the moment it is difficult for me to speculate about this finding. However, single X-ray analysis showed that despite indications of orientational order these samples behave as poly crystalline aggregates.

2.6 Concluding remarks

This thesis explored the structure of amorphous calcium carbonate synthesized via additive free mixing of solutions at constant pH values. We demonstrated by using different characterization techniques that the amorphous calcium carbonate have short range orders, which are similar to the crystalline phases of calcium carbonate. The nano-particles of the amorphous phase seem to be consisted of smaller nano-particles, which suggested an aggregation mediated nucleation on the formation of the amorphous phase. Further more, the effect of experimental conditions in the crystallization of calcium carbonate was investigated. Stirring rate showed a strong influence in the kinetic stabilization of the metastable phase vaterite, both with and without additive. Also here, an aggregation mediated mechanism was hypothesized to cause the observed behaviour. With additive in solution effects of temperature, pH and polymer concentration were investigated. Interesting morphologies were obtained which has been attributed to the effect of specific additives in literature. We showed that the combinational effect of the additive and experimental condition resulted in such morphologies.

Summary and future outlook

CO_2 capture has no unique solution so far and constitutes a complex challenge that certainly requires integration of several technologies. Apart from the politic-economical challenges, a key factor in the technical-economical aspect lies in improved materials that perform the separations. A promising material should significantly lower the cost for carbon capture. It should possess properties such as high capturing capacity, high selectivity, thermal and mechanical stability, be easily regenerated and recyclable. How to combine these rather conflicting properties is a challenge that needs extensive studies and input from many fields of science and engineering. Multifunctional materials hold great promise as the different functions can be optimized separately. In this thesis, amine modified porous silica can be considered as such a material. We combined mechanical and thermal stability of porous silica with excellent interaction properties of propylamine groups with CO_2. We determined that chemisorption is the dominant process in the carbon capture at partial pressures of CO_2 in flue gas and also different surface densities of amine groups on the surface can be obtained by adjusting the modification parameters. Of course further investigations will be needed before considering using amine modified silica in carbon capture applications. One could also explore the possibility to use amine modification on another kind of substrate. For example carbonaceous adsorbents which are mainly used in precombustion capture, such as activated carbon possess excellent properties such as heat transfer, moisture insensitivity and less expensive compared to zeolites and porous silica. Amine modification of these substrates will allow them to be used in low temperature postcombustion capture.

In the second part of this thesis, crystallization of calcium carbonate was investigated. We determined that amorphous calcium carbonate can have short range order similar to the subsequent crystalline phase, namely calcite and vaterite. We explained that crystallization of calcium

carbonate occurs through an aggregation mediated mechanism and determined how it depends on experimental conditions. The increased knowledge about the precipitation of calcium carbonate will certainly help to design new materials for carbon capture. A multifunctional material consisting of calcium carbonate and a thermally stable compound will certainly be advantageous as compared with pure calcium carbonate. A key could be in synthesizing very small calcium carbonate particles embedded in a network of a thermally stable compound. In this way problems related to the sintering of particles and the gas-solid diffusion could be eliminated and one would end up with a multifunctional CO_2 sorbent partially based on the $CaO/CaOH\text{-}CaCO_3$ cycle. Clearly, the knowledge from crystallization of calcium carbonate could enable construction of high temperature sorbents for CO_2.

2.7 References

(1) Ridgwell, A.; Zeebe, R. E. *Earth planet. Sci. Lett.* **2005**, *234*, 299–315.
(2) Chan, C. M.; Wu, J. S.; Li, J. X.; Cheung, Y. K. *Polymer* **2002**, *43*, 2981–2992.
(3) Domb, A. J.; Manor, N.; Elmalak, O. *Biomaterials* **1996**, *17*, 411–417.
(4) Gascho, G. J.; Parker, M. B. *Agron.J.* **2001**, *93*, 1305–1315.
(5) Lemos, A. F.; Ferreira, J. M. F. *Mater. Sci. Eng., C* **2000**, *11*, 35–40.
(6) Pera, J.; Husson, S.; Guilhot, B. *Cem.Concr.Compos.* **1999**, *21*, 99–105.
(7) Wei, W.; Ma, G.-H.; Hu, G.; Yu, D.; Mcleish, T.; Su, Z.-G.; Shen, Z.-Y. *J.Am.Chem.Soc.* **2008**, *130*, 15808–+.
(8) Falini, G.; Albeck, S.; Weiner, S.; Addadi, L. *Science* **1996**, *271*, 67–69.
(9) Aizenberg, J.; Hanson, J.; Ilan, M.; Leiserowitz, L.; Koetzle, T. F.; Addadi, L.; Weiner, S. *Faseb J.* **1995**, *9*, 262–268.
(10) Gehrke, N.; Nassif, N.; Pinna, N.; Antonietti, M.; Gupta, H. S.; Colfen, H. *Chem. Mater.* **2005**, *17*, 6514–6516.
(11) Addadi, L.; Weiner, S. *Angew. Chem. Int. Ed.* **1992**, *31*, 153–169.
(12) Meldrum, F. C.; Coelfen, H. *Chem.Rev.* **2008**, *108*, 4332–4432.
(13) Meldrum, F. C. *Int. Mater. Rev.* **2003**, *48*, 187–224.
(14) Beniash, E.; Aizenberg, J.; Addadi, L.; Weiner, S. *Proc. R. Soc. Lond. Ser. B-Biol. Sci.* **1997**, *264*, 461–465.
(15) Radha, A. V.; Forbes, T. Z.; Killian, C. E.; Gilbert, P. U. P. A.; Navrotsky, A. *Proc. Natl. Acad. Sci.* **2010**, *107*, 16438–16443.
(16) Rodriguez-Blanco, J. D.; Shaw, S.; Benning, L. G. *Nanoscale* **2011**, *3*, 265–271.
(17) Bolze, J.; Peng, B.; Dingenouts, N.; Panine, P.; Narayanan, T.; Ballauff, M. *Langmuir* **2002**, *18*, 8364–8369.
(18) Liu, J.; Rieger, J.; Huber, K. *Langmuir* **2008**, *24*, 8262–8271.
(19) Coelfen, H.; Antonietti, M. *Mesocrystals and Nonclassical Crystallization*; John Wiley and Sons, 2008.
(20) Gower, L.; Odom, D. *J. Cryst. Growth* **2000**, *210*, 719–734.
(21) Gebauer, D.; Voelkel, A.; Coelfen, H. *Science* **2008**, *322*, 1819–1822.
(22) Demichelis, R.; Raiteri, P.; Gale, J. D.; Quigley, D.; Gebauer, D. *Nat. Commun.* **2011**, *2*, 590.
(23) Van Santen, R. A. *J. Phys. Chem.* **1984**, *88*, 5768–5769.
(24) Threlfall, T. *Org. Process Res. Dev.* **2003**, *7*, 1017–1027.

(25) Levi-Kalisman, Y.; Raz, S.; Weiner, S.; Addadi, L.; Sagi, I. *Adv. Funct. Mater.* **2002**, *12*, 43–48.
(26) Raz, S.; Testeniere, O.; Hecker, A.; Weiner, S.; Luquet, G. *Biol. Bull.* **2002**, *203*, 269–274.
(27) Aizenberg, J.; Lambert, G.; Weiner, S.; Addadi, L. *J.Am.Chem.Soc.* **2002**, *124*, 32–39.
(28) Raz, S.; Hamilton, P.; Wilt, F.; Weiner, S.; Addadi, L. *Adv. Funct. Mater.* **2003**, *13*, 480–486.
(29) Gower, L. A.; Tirrell, D. A. *J. Cryst. Growth* **1998**, *191*, 153–160.
(30) Huang, S.-C.; Naka, K.; Chujo, Y. *Langmuir* **2007**, *23*, 12086–12095.
(31) Colfen, H.; Qi, L. M. *Chem. Eur. J.* **2001**, *7*, 106–116.
(32) Gorna, K.; Hund, M.; Vucak, M.; Groehn, F.; Wegner, G. *Mater. Sci. Eng.* **2008**, *477*, 217–225.
(33) Xu, AW; Yu, Q.; Dong, W.F.; Antonietti, M.; Cölfen, H. *Adv. Mater.* **2005**, *17*, 2217–2221.
(34) Lam, R. S. K.; Charnock, J. M.; Lennie, A.; Meldrum, F. C. *Crystengcomm* **2007**, *9*, 1226–1236.
(35) Politi, Y.; Levi-Kalisman, Y.; Raz, S.; Wilt, F.; Addadi, L.; Weiner, S.; Sagi, I. *Adv. Funct. Mater.* **2006**, *16*, 1289–1298.
(36) Hasse, B.; Ehrenberg, H.; Marxen, J. C.; Becker, W.; Epple, M. *Chem. Eur. J.* **2000**, *6*, 3679–3685.
(37) Brecevic, L.; Nielsen, A. E. *J .Cryst .Growth* **1989**, *98*, 504–510.
(38) Loste, E.; Meldrum, F. *Chem. Commun.* **2001**, 901–902.
(39) Colfen, H. *Curr. Opin. Colloid Interface Sci.* **2003**, *8*, 23–31.
(40) Ren, D.; Feng, Q.; Bourrat, X. *Micron* **2011**, *42*, 228–245.
(41) Gebauer, D.; Coelfen, H.; Verch, A.; Antonietti, M. *Adv. Mater.* **2009**, *21*, 435–+.
(42) A novel view on the early stage of crystallization http://opus.kobv.de/ubp/volltexte/2008/1981/ (accessed Mar 22, 2012).
(43) Gunther, C.; Becker, A.; Wolf, G.; Epple, M. *Z. Anorg. Allg. Chem.* **2005**, *631*, 2830–2835.
(44) Loste, E.; Wilson, R.; Seshadri, R.; Meldrum, F. *J. Cryst. Growth* **2003**, *254*, 206–218.
(45) Aizenberg, J.; Lambert, G.; Addadi, L.; Weiner, S. *Adv. Mater.* **1996**, *8*, 222–&.
(46) Kojima, Y.; Kawanobe, A.; Yasue, T.; Arai, Y. *J. Ceram. Soc. Jpn.* **1993**, *101*, 1145–1152.
(47) Sondi, I.; Skapin, S. D.; Jurina, I.; Slovenec, D. *Geol. Croat.* **2011**, *64*, 61–65.
(48) Turnbull, A. G. *Geochim. Cosmochim. Acta* **1973**, *37*, 1593–1601.
(49) Yao, Y.; Dong, W.; Zhu, S.; Yu, X.; Yan, D. *Langmuir* **2009**, *25*, 13238–13243.

(50) Xu, A. W.; Antonietti, M.; Colfen, H.; Fang, Y. P. *Adv. Funct. Mater.* **2006**, *16*, 903–908.
(51) Wang, T.; Antonietti, M.; Colfen, H. *Chem. Eur. J.* **2006**, *12*, 5722–5730.
(52) Oaki, Y.; Kajiyama, S.; Nishimura, T.; Imai, H.; Kato, T. *Adv. Mater.* **2008**, *9999*, NA.
(53) Qi, L.; Colfen, H.; Antonietti, M.; Li, M.; Hopwood, J.; Ashley, A.; Mann, S. *Chem. Eur. J.* **2001**, *7*, 3526–3532.

Acknowledgements

I would like to thank a number of people for all the help and support during this thesis.

Niklas, my supervisor, there is no word that can describe my deepest gratitude. I guess that I was the luckiest PhD student to have you not only as my supervisor but also as a friend, I appreciate that no matter how stressed you were sometimes, I could knock at your door and ask questions. I have learned many things from you including old Swedish words ☺. You have been great, thanks! I want also to thank my co-supervisor Lennart Bergström for all the things that I've learned and all your help during these five years.

I would like to thank my colleges Dr Zoltan Bacsik, Dr Denis Gebauer and Dr Guoying Zhao for nice collaborations. It has been a pleasure to work with you and learn so much from you. Zoltan I appreciate the sweet Hungarian language when experiments fail.

I wish to thank everyone at the department of MMK for very nice and friendly atmosphere. Special thanks goes to administrative staff, to the workshop guys Pelle and Hans Erik, Roffe for his computer help and to Hillevi for all the library helps. I would like to thank Dr. Kjell Jansson for all the help in electron microscopy and thermal analysis. I thank Dr Alessandra Quadrelli for all things that I learned in France in oxygen and water free synthesis and for her nice Risotto when I was at hospital there.

I would like to thank people in YKI and specially those of CODIRECT for all the nice presentations and ideas. Also CODIRECT for financing this project.

I want also to thank all my friends at MMK for being there and making the life fun. Neda, for being a dear and kind friend, for all the lunches and your excellent Persian food. I wish you all the best and success during your PhD time. Ehsan my dear friend and Jovice for all the laughs

and good times. German and Marta for all the jokes and being Barca fan. Bertrand, Farid, Mia, Samrand, Ocean, Orlando and your kind wife, Christina, Wenming and Mikaela thanks for the tips. My former roommate Linnea and current ones Arto, Erik and Arnaud thanks for reading my thesis. All the friends outside MMK that made my days easier for being there, Mahsa, Maryam Ali, Mahan and all of the others who I forgot.

Last but not least I would like to thank each and every member of my family. In particular my father and mother for spending their life in struggle for Kurdistan's freedom. I am grateful for all the love and encouragements that you gave me even when the life was hard.

Sopas babo, dayê bû hemî ew zehmetên we kişay li van salêt borî. Ez heta heta deyndarî weme. Sopas bû hevjina min Sabre bo ew zehmata te kêşay o ew tehemola te di gel min borandi. Sopas bû biçîkên min Helin û Diyako û Chiavan bo ronahi kirina jîana min. Sopas bû xûşk û birayêt min Nizar û Pershin o biçîkên we, Jîan û Isamil û her dû biçîkên we Roya o Raman Tarash û biçîkên te çinar o kiça te ya delal Rosa. Mazin o Mehe û biçîkên we. Hezni o Avin o Bishang her wesa Hevali. Sopas bo hemi malo miroven min o hevalen min. Hîvîdarim her dem sax o silamet bin.